International Journal of Biological Macromolecules 298 (2025) 139621

Contents lists available at ScienceDirect

International Journal of Biological Macromolecules

journal homepage: www.elsevier.com/locate/ijbiomac

# Synthesis, biological evaluation and molecular docking studies of flavonol-3-*O*-β-D-glycoside as a potential inhibitor of SARS-CoV-2 main protease (3CLpro) in drug development for COVID-19

Gonca Çelik [a,*], Şengül Alpay Karaoğlu [b], Şeyma Suyabatmaz [b], Arif Bozdeveci [b], Gizem Tatar Yılmaz [c,d,e], Nurettin Yaylı [f], Rahşan Akpınar [g], Ayşegül Çopur Çiçek [h]

[a] Department of Chemistry, Faculty of Science, Karadeniz Technical University, Trabzon 61080, Türkiye
[b] Department of Biology, Faculty of Science, Recep Tayyip Erdoğan University, Rize 53100, Türkiye
[c] Department of Biostatistics and Medical Informatics, Faculty of Medicine, Karadeniz Technical University, Trabzon 61080, Türkiye
[d] Karadeniz Technical University, Institute of Health Sciences, Department of Bioinformatics, 61080 Trabzon, Türkiye
[e] Yılmaz Bilişim R&D Consulting Software Engineering and Services Trade Limited Company, 61081 Trabzon, Türkiye
[f] Department of Pharmacognosy, Faculty of Pharmacy, Karadeniz Technical University, Trabzon 61080, Türkiye
[g] Laboratory of Bee Diseases, Samsun Veterinary Control Institute, Samsun 55200, Türkiye
[h] Department of Basic Medical Sciences, Faculty of Medicine, Istanbul Medipol University, Istanbul 34815, Türkiye

ARTICLE INFO

*Keywords:*
Flavonol-3-*O*-glycoside
SARS-CoV-2
COVID-19
Nuclease activity
Antimicrobial activity
Molecular docking

ABSTRACT

The COVID-19 pandemic began in March 2020 and has affected many countries and infected over a million people. It has had a serious impact on people's physical and mental health, daily life and the global economy. Today, many drugs show limited efficacy in the treatment of COVID-19 and studies to develop effective drugs continue. Here, we aim to the synthesise and characterise of the flavonol-3-*O*-glycoside derivatives, the following and evaluated molecular docking studies with antimicrobial activity, inhibition of SARS-CoV-2 main protease enzyme (3CLpro) and nuclease activity. Molecular docking simulations of the synthesized flavonol-3-O-glycoside derivatives, especially compounds **5a, 5d, 5h, 5i** and **5m,** showed a stronger interaction with SARS-CoV-2 3CLpro in the active site. Two compounds from the target compounds, **5h** and **5m**, were found to be specifically effective against *M. smegmatis* and yeasts. In particular, compounds **5a, 5d, 5h, 5i** and **5m**, which exhibited high activity against the SARS-CoV-2 main protease enzyme, were found to be effective at low concentrations. We determined the $IC_{50}$ values for the compounds that showed an inhibitory effect as well as their nuclease activities, which further emphasising the potential of our results. Among these, compound **5d** showed a significant competitive inhibitor of 3CLpro. Furthermore, nuclease activity studies identified compound **5d** as the most potent. The above results suggest that the flavonol-3-*O*-glycoside derivatives could be promising new antiviral agents for the development of 3CLpro inhibitors to combat COVID-19.

## 1. Introduction

A novel strain of the extremely contagious pathogenic coronavirus disease 2019 (COVID-19), caused by the acute respiratory syndrome coronavirus SARS-CoV-2 [1]. SARS-CoV-2 is a positive-sense and single-stranded ribonucleic acid (+ssRNA) virus that leads to a severe acute respiratory syndrome such as pneumonia and respiratory failure [2–4]. In addition SARS-CoV-2 enters the host cell and contains a receptor-binding domain of the spike protein (S protein) that binds to angiotensin-converting enzyme 2 (ACE2), which determines human transmissibility and inflammatory response [1,5–6].

In December 2019, an outbreak began in Wuhan, China, and quickly spread around the world. On March 11, 2020, the World Health Organization (WHO) declared the COVID-19 pandemic [4]. According to the WHO Coronavirus (COVID-19) Dashboard, there have been >7 million deaths and >776 million infected cases worldwide as of October 2024 [7].

The coronaviruses are divided into types of strains such as α-coronavirus (α-CoV), β-coronavirus (β-CoV), γ-coronavirus (γ-CoV), δ-coronavirus (δ-CoV) [8]. The SARS-CoV-2 virus belongs to the genus β-CoV

* Corresponding author at: Department of Chemistry, Faculty of Science, Karadeniz Technical University, 61080 Trabzon, Turkey.
*E-mail address:* mavi_gnc@hotmail.com (G. Çelik).

https://doi.org/10.1016/j.ijbiomac.2025.139621
Received 7 November 2024; Received in revised form 6 January 2025; Accepted 6 January 2025
Available online 14 January 2025

genus, and posses a serious threat to human health [9,10]. Studies have shown the that symptoms are fever, dry cough, fatigue, body aches and pains, stuffy nose, headache, conjunctivitis, sore throat, diarrhea, loss of taste or smell, rash or discoloration of the fingers on the hand in this disease [11–14].

The β-CoV genome encodes four major structural proteins (S: spike; E: envelope; M: membrane; N: nucleocapsid), and several non-structural proteins (nsps), including the coronavirus main protease ($M^{pro}$) or also known as 3-chymotrypsn-like protease ($3CL^{pro}$), the RNA-Dependent RNA polymerase (RdRp) and the papain-like protease ($PL^{pro}$) [15–18]. And although the $3CL^{pro}$ and its homolog is an ideal target for the screening and development of anti-SARS-CoV-2 drugs [19,20]. To date, some antiviral, antimalarial and immunomodulatory drugs such as remdesivir, chloroquine, hydroxychloroquine, flavipiravir, tilorone and umifenovir have been used. Further studies have shown that there are no specific and safe antiviral drugs that have been researched for the treatment of COVID-19 infections [21–26].

Flavonols (3-hydroxyflavones) are the most active compounds of the flavonoid family, exibiting potent pharmacological activities, including antimicrobial, antioxidant and anticancer effects and good biocompatibility [27,28]. They are mainly found in vegetables, beverages, fruits, flowers, bark, seeds and nuts [29,30]. Particularly, quercetin (3, 3, 4, 5, 7-pentahydroxyflavone) is a polyhydroxy compounds a natural subclass of flavanols with high medicinal value including health benefits. Quercetin and quercetin derivatives are present in their natural form as glycosides with different sugar units, which are more stable and soluble and usually have excellent biological activities [31–33]. As recent studies have shown, quercetin-glycoside derivatives have been tested for their antimicrobial activity and showed significant activity [34,35]. In addition, research has reported that quercetin-3-β-galactoside reduces the activity of SARS-CoV-$3CL^{pro}$ [36]. Quercetin-3-*O*-glycoside is an excellent compound that binds to the $M^{pro}$ enzyme, and can thus be considered a COVID-19 drug *via* the inhibition of SARS-CoV-2 activities (Fig. 1) [37].

As far as we know there is not much literature available on the flavonol-3-*O*-glycosides of SARS-CoV-2 inhibitors, except for a few examples [33,36]. Based on these previous findings, we hypothesized that flavonol-3-*O*-glycoside could inhibit the 3CLpro activity of SARS-CoV-2. In the following, the synthesis, structural characterization and molecular docking studies as well as the antimicrobial activity, the inhibition of the SARS-CoV-2 main protease enzyme (3CLpro) and the nuclease activity are investigated in detail.

## 2. Results and discussion

### 2.1. Chemistry

In this work, the structurally diverse synthetic pathway of the target compounds flavonol-3-*O*-glycoside (**5a–r**) is illustrated as in Scheme 1. Flavonol-3-*O*-glycosides (**5a–r**) were synthesized from substituted aromatic ketones (**1**) and substituted aromatic aldehydes (**2**) in three steps. Previously, we synthesized a series of chalcone derivatives (**3a–r**) using the well-established base-catalyzed Claisen-Schmidt condensation, which gives good yields [38]. These chalcone derivatives (**3a–r**) were then oxidatively cyclized with 35 % hydrogen peroxide ($H_2O_2$) to obtain flavonol derivatives (**4a–r**) in moderate to excellent yields by the Algar-Flynn-Oyamada (AFO) reaction [39,40]. Finally, the 3-*O*-glycoside of flavonols was synthesized with 2,3,4,6-tetra-*O*-acetyl-α-D-glucopyranosyl bromide (TAGBr) in dry acetone under inert atmosphere to obtain acetylflavonols. Deacetylated reactions take place with $NaOCH_3$ in dry methanol according to the Zemplen method to obtain the target flavonol-3-*O*-glycosides in moderate yields (**5a–r**) [41,42]. Based on the relevant literature, compounds **3a–i, 3k, 3l, 3o, 3r, 4a–i, 4o, 5c** and **5f** have been described so far [43–46]. To the best of our knowledge, all other compounds **3j, 3m, 3n, 3p, 3q, 4j–n, 4p–r, 5a, 5b, 5d, 5e, 5g, 5h, 5i** and **5j–r** are new. Subsequently, the structure of all compounds was established by analysing the IR, $^1$H NMR, $^{13}$C NMR and HRMS spectroscopy methods.

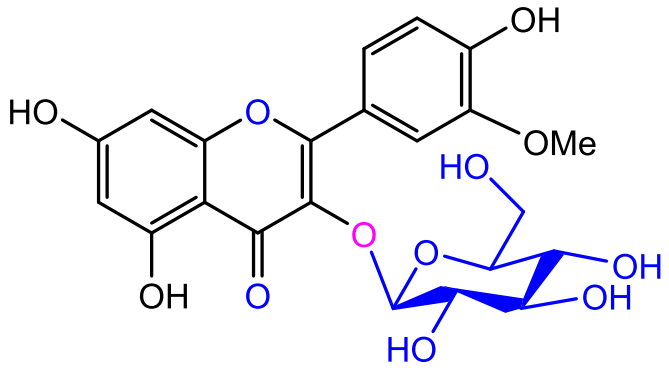


**Fig. 1.** Representative structure of quercetin-3-*O*-glycoside.

The IR spectrum of the chalcone compounds (**3a–r**) showed peaks around of 3100 $cm^{-1}$ attributable to 2′-OH, 1638 $cm^{-1}$ attributable to C═O and 1565 $cm^{-1}$ attributable to C═C. The flavonol compounds (**4a–r**) showed the absoprtion IR peaks at 3241–3315 $cm^{-1}$ (3-OH stretching), 1598–1613 $cm^{-1}$ (C═O stretching) and 1155–1210 $cm^{-1}$ (C—O stretching), respectively. The characteristic peaks for the O-β-D-glucosyl skeletal linkage (glucosidic C—H stretching) were found at 2939–2968 $cm^{-1}$ for flavonol-3-*O*-glycoside compounds (**5a–r**). Similarly, the β-configuration of anomeric carbon stretching for flavonol-3-*O*-glycoside was observed at 842–908 $cm^{-1}$ [42,47].

The $^1$H NMR spectra of the chalcone compounds (**3a–r**) show two characteristic doublets at ~7.7 ppm (d, $J$ = ~15.4 Hz, 1H, H-2, A part of the AB system) and ~7.99 ppm (d, $J$ = ~15.4 Hz, 1H, H-3, B part of the AB system) corresponding to the olefinic proton in the enone bond in the chalcone molecule. In addition, the $J$ value (1H—1H coupling constant) of 15.4 Hz confirmed the formation of the E configuration of the olefinic proton in the chalcone molecule (**3j**) (see electronic Supplementary Information (ESI) for details) [48]. In addition, compound **3j** contains a hydroxy group at the H-2′ position, as shown by the resonance signal at $\delta_C$ 13.17 ppm (s, 1H) in the NMR spectra. The flavonol skeleton was confirmed by the $^1$H NMR signals at $\delta_H$ 8.14 (d, $J$ = 7.5 Hz, 1H, H-5), $\delta_H$ 7.19 (t, $J$ = 8.6 Hz, 1H, H-6), $\delta_H$ 7.47 (m, 1H, H-8) and $\delta_H$ 8.45 (s, 1H, 3-OH) for compound **4n** (see ESI) [49]. For all flavonol-3-*O*-glycoside compounds (**5a–r**), the $^1$H NMR spectra show a doublet signal at $\delta_H$ 4.92–5.54 ($J$ = ~7.4 Hz) confirming the β-orientation of the sugar moiety. That this also demonstrated the glupyranosyl group was bound to the C-3 position. Furthermore, the D-glucose unit was in the β-orientation, which was confirmed by a positive value as the D-configuration [50]. Thus, the structure of compounds (**5a–r**) was elucidated as flavonol-3-*O*-β-D-glycoside. As well, $^1$H NMR (400 MHz, DMSO/$CDCl_3$) spectrum of **5l** shows multiplet signals (6H) around $\delta$ 3.0–3.6 ppm assignable for the glucosidic proton of the flavonol-3-*O*-glycoside beside the signals corresponding to the glucosidic OH in the region $\delta_H$ 4.2–5.5 ppm. Furthermore, the $^1$H spectra for all compounds (**3a–r, 4a–r** and **5a–r**) showed the protons of the aromatic ring in the range of 6.69–8.30 ppm, indicating the expected chemical shifts and integral values.

The $^{13}$C NMR of compounds (**3a–r**) showed diagnostic peaks of the three $sp^2$ quaternary hybridized carbon atoms with chemical shifts at $\delta_C$ ~192.0 (including a carbonyl carbon), $\delta_C$ ~122.0 ppm (C-2) and $\delta_C$ ~143.0 (C-3) ppm, confirming the connectivity of the carbon skeleton [51]. In agreement with the $^{13}$C NMR spectrum of the flavonol compounds (**4a–r**), three carbon sequence of $\delta_C$ ~144.0 (C-2), $\delta_C$ ~138.0 (C-3) and $\delta_C$ ~172.0 (including carbonyl carbon) ppm were revealed [52]. Based on the above analysis, the planar structure of flavonol was determined. In addition, the $^{13}$C NMR spectrum of the compounds (**5a–r**) showed only one peak at $\delta_C$ ~102.0 ppm, confirming that the β-D-glucose moiety was also bound to the C-3 position [42,47,50,53]. Therefore, the structure of **5a–r** was elucidated as a flavonol-3-*O*-β-D-

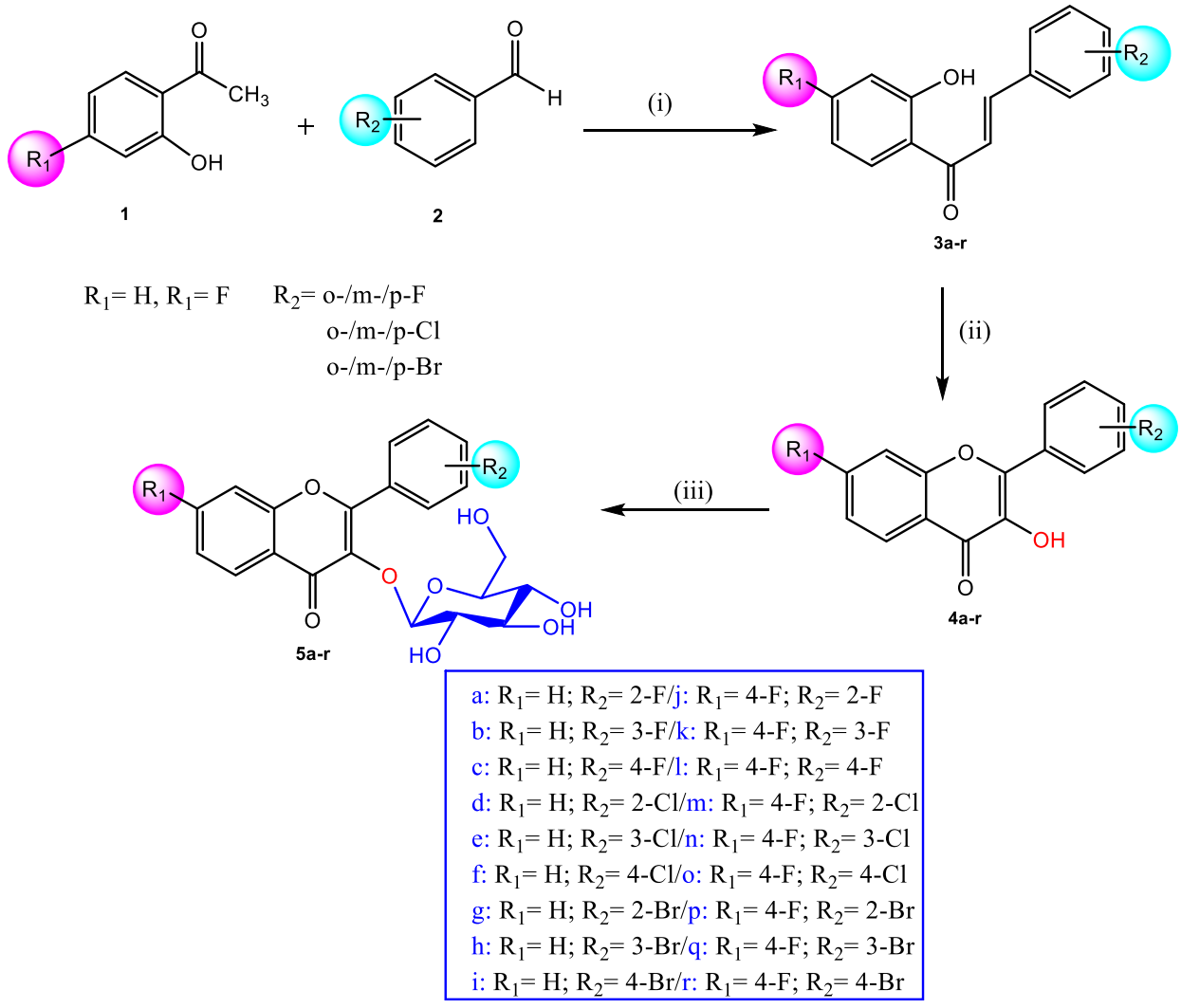


**Scheme 1.** General ways to produce the target compounds **5a–r**. Reagents and conditions: i: 40 % KOH, ethanol, rt); ii: $Na_2CO_3$, 35 % $H_2O_2$, methanol); iii: Acetone, TAGBr, methanol, KOH, 0–5 °C, $NaOCH_3$, methanol).

glycoside. The characteristic glucosidic and aromatic ring carbons were located at the expected chemical shifts for the compounds (**5a–r**). Another interesting feature of the fluorine-substituted compounds is that the fluorine carbon signals in the $^{13}C$ NMR spectra are magnetically inequivalent, although they are not diastereotopic. Consequently, in the $^{13}C$ NMR (100 MHz, DMSO/$CDCl_3$) spectra of compound **5j**, the characteristic carbon-fluorine signals were found to be doublets at $\delta_C$ 128.42/128.31 (C-5, $^3J_{CF}$= 11 Hz), 114.28/114.05 (C-6, $^2J_{CF}$ = 23 Hz), 167.07/164.60 (C-7, $^1J_{CF}$= 252 Hz), 105.07/104.81 (C-8, $^2J_{CF}$ = 26 Hz), 156.83/156.69 (C-9, $^3J_{CF}$ = 14 Hz), 120.93 (C-10), 118.99/118.85 (C-1′, $^2J_{CF}$ = 14 Hz), 161.22/158.72 (C-2′, $^1J_{CF}$ = 250 Hz),115.90/115.69 (C-3′, $^2J_{CF}$ = 21 Hz), 133.02/132.93 (C-4′, $^3J_{CF}$ = 9 Hz), 124.09/125.05 (C-5′, $^4J_{CF}$ = 4 Hz),132.33/132.30 (C-6′, $^3J_{CF}$ = 3 Hz) ppm (see ESI) [38,53].

Finally, the mass spectra of all synthesized compounds (**3a–r, 4a–r** and **5a–r**) showed molecular ion peaks at the corresponding *m/z* values, confirming their molecular mass. Compound **3j** is a yellow solid, and its molecular formula was determined to be $C_{15}H_{10}F_2O_2$ based on HRMS for the peak at *m/z* 261.0722 [M + H]+ (calc. for $C_{15}H_{10}F_2O_2$, 261.0649). In addition, compound **4j** was obtained as a yellow solid, and its molecular formula was determined by HRMS for the peak at *m/z* 275.0473 [M + H]+ (calc. for $C_{15}H_8F_2O_3$, 275.219) as $C_{15}H_8F_2O_3$. In addition, compound **5l** was obtained as a pale yellow powder and HRMS showed an $[M + H]^+$ ion peak at 437.1008 *m/z*, which gave the molecular formula $C_{21}H_{18}F_2O_8$ (calc. for $C_{21}H_{18}F_2O_8$, 437.0970) (see ESI).

## 2.2. Molecular modeling study

### 2.2.1. Molecular docking results

This study, we used the SARS-CoV-2 3CLpro crystal structure in complex with the N3 inhibitor for molecular docking analysis. First, redocking was performed with this reference compound N3 in the crystal structure to validate the docking simulations (Fig. 2). This compound formed pi-sigma interactions with His41, pi-sulfur with Met165, alkyl interactions with Leu141, pi-alkyl interactions with His163 and His164, and hydrogen bonding interactions with Glu166, Arg188, Thr190, and Gln189 (Fig. 2).

After the validation process, we investigated the binding mechanisms between the flavonol-3-*O*-glycosides and the SARS-CoV-2 3CLpro enzyme at the molecular level and predicted their binding affinities. All synthesized compounds **(5a–r)** showed significant inhibitory effects on SARS-CoV-2 3CLpro and outperformed the reference inhibitor N3. *In vitro* analysis revealed that compounds **5a, 5m, 5h, 5i** and **5d** exhibited the strongest activity, with inhibitory concentrations of 8.42 μM, 14.56 μM, 14.85 μM, 16.11 μM and 18.06 μM, respectively. These compounds also showed stronger binding affinities in the docking study (see Table 1).

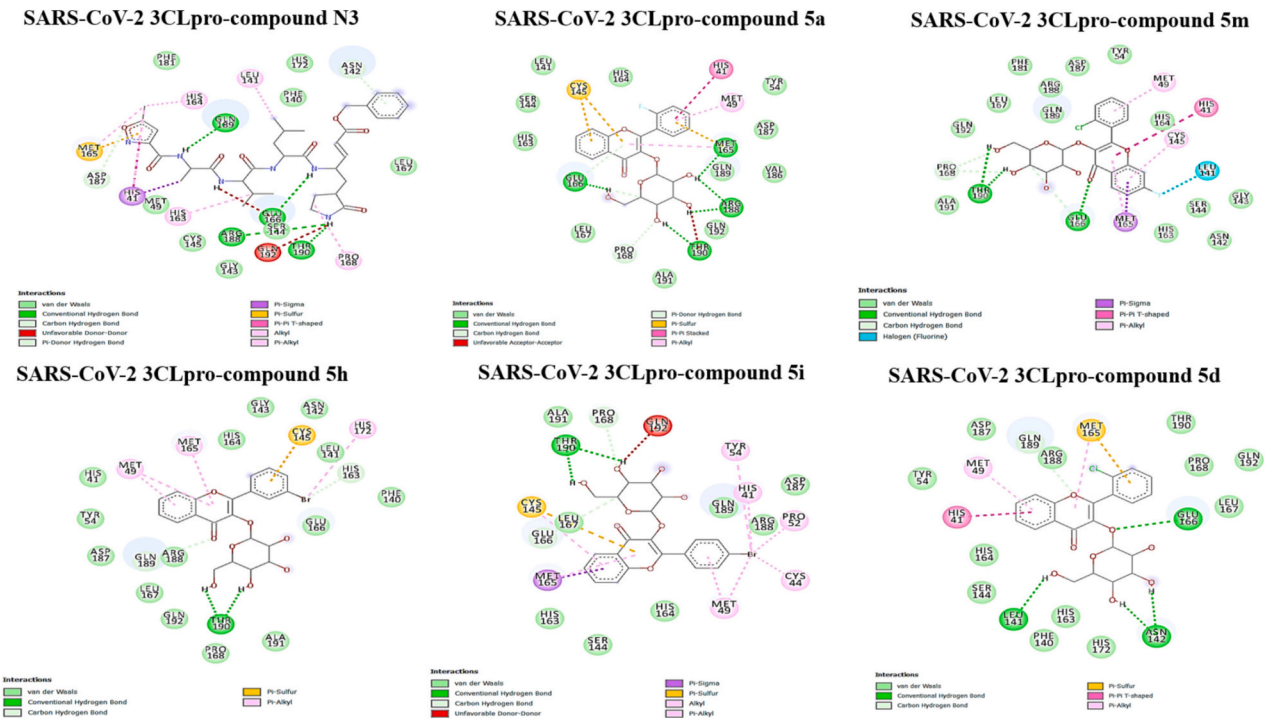


**Fig. 2.** The 2D analysis of the binding conformations with the lowest energy of the SARS-CoV-2 3CLpro enzyme with the active compounds.

**Table 1**
As a result of docking analysis of flavonol-3-*O*-glycoside (**5a–r**) and N3 (reference) compounds, the lowest binding energy values in the active site of SARS-CoV-2 3CL$^{pro}$.

| Compounds | Binding energy (kcal/mol) |
|---|---|
| **5a** | −9.13 |
| **5b** | −8.65 |
| **5c** | −8.55 |
| **5d** | −8.80 |
| **5e** | −9.10 |
| **5f** | −9.44 |
| **5g** | −9.36 |
| **5h** | −9.31 |
| **5i** | −9.42 |
| **5j** | −8.62 |
| **5k** | −8.54 |
| **5l** | −8.84 |
| **5m** | −9.11 |
| **5n** | −9.25 |
| **5o** | −9.80 |
| **5p** | −9.30 |
| **5q** | −9.41 |
| **5r** | −10.10 |
| Reference compound (N3) | −8.31 |

Compound **5a**, which has the highest binding affinity to the SARS-CoV-2 3CLpro enzyme, forms a hydrogen bond with the amino acid Glu166, Thr190, Met165 and Arg188, a π-sulfur bond with the amino acid Cys145, a π–alkyl with Met49, a van der Waals bond with Leu141, Ser144, His163, Leu167, Ala191, Gln192, Val186, Asp187, Tyr54 and Asp187 of SARS-CoV-2 3CLpro (Fig. 2). The other active compounds interacted mainly with the SARS-CoV-2 3CLpro enzyme through hydrogen bond interactions with residues Met165, Glu166, Gln189, Thr190, Asn142, and Leu141, similar to the interactions observed with crystallized compound N3 (see Fig. 2). These residues are located in the catalytic region of the enzyme and are highly conserved among SARS-CoVs [54,55], indicating their key role in binding affinity. This information will help us develop more effective antiviral drugs for COVID-19.

### 2.2.2. *Molecular dynamic simulations results*

Molecular dynamics (MD) simulation is a computational technique widely used to model the dynamic behavior of molecular systems over time. This method enables the evaluation of the stability and binding affinity of protein-ligand complexes by simulating their atomic-level interactions [56]. In this study, molecular dynamics (MD) simulations were conducted using the Desmond software package to evaluate the binding affinity and stability of the hit compound **5a** and a reference compound against the SARS-CoV-2 3CLpro target over a 100-ns simulation period.

To assess the overall structural stability of the target protein in complex with the tested compounds, root mean square deviation (RMSD) analysis was carried out. This analysis provides valuable insights into the extent of structural deviation from the initial conformation throughout the simulation. For the SARS-CoV-2 3CLpro protein, RMSD values for Cα atoms were observed in the range of 1.1 to 4.9 Å with compound **5a** and 0.9 to 2.9 Å with the reference compound (Fig. 3A). Additionally, root mean square fluctuation (RMSF) values were analyzed to evaluate the flexibility of individual protein residues in the presence of the tested compounds. As depicted in Fig. 3B, residues interacting (marked by green vertical bars) with compound **5a** and the reference compound exhibited RMSF values ranging from 0.6 to 3.5 Å.

The non-covalent interactions between the protein and ligands were monitored throughout the simulation to understand the binding affinity of the hit compounds and the stability of their conformations within the active site. His41, Met165, His163, His164, Glu166, Arg188, Thr190, and Gln189, key residues known to play essential roles in the catalytic activity of SARS-CoV-2 3CLpro [54,55], were observed to maintain hydrogen bonding, hydrophobic interactions, and ionic interactions with both compound **5a** and the reference compound throughout the simulation (Fig. 3C). These findings suggest stable interactions between the ligands and the catalytic domains of SARS-CoV-2 3CLpro, further supporting their strong binding affinity, as confirmed by RMSD and RMSF analyses.

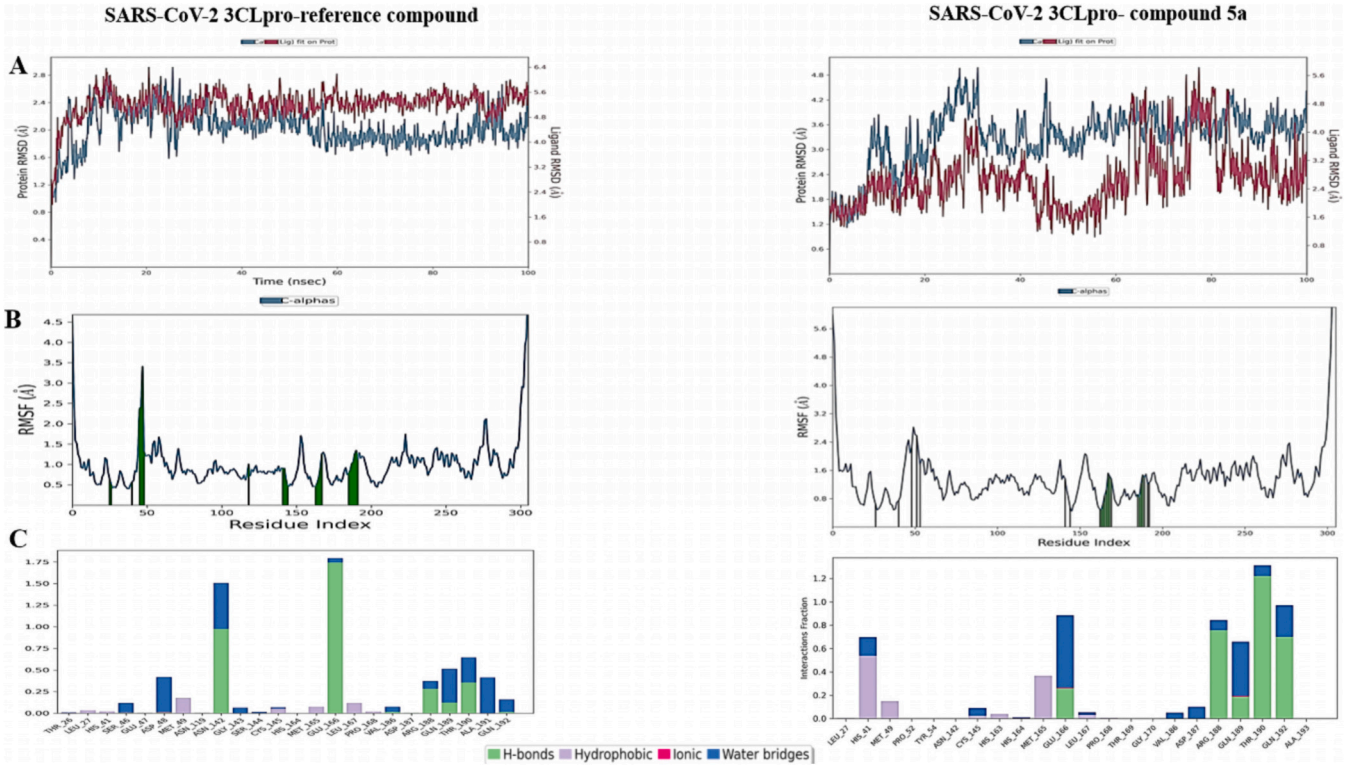


**Fig. 3.** (A) The RMSD calculation, represented by the blue line for the protein and the red line for the ligand, was conducted for each complex (SARS-CoV-2 3CLpro/compound) during the 100 ns MD simulation. (B) The RMSF assessment was performed for each complex (SARS-CoV-2 3CLpro/compound) following a 100 ns MD simulation. (C) The four main factors in protein-ligand interaction are hydrogen bonds, hydrophobic contacts, ionic interactions, and water bridges. Stacked bar graphs visualize these interactions throughout the trajectory, indicating the duration as a percentage of simulation time.

### *2.3. Biological evaluation*

#### *2.3.1. Antimicrobial properties of the target compounds*

In the study, the minimum inhibitory concentration (MIC) method was used against selected pathogenic indicator microorganisms to determine the antimicrobial activity properties of the compounds. In the study, antimicrobial activity against nine microorganisms was tested on various pathogenic bacteria and fungi suitable for human consumption.

The antimicrobial activities of the substances were analyzed using the MIC method. In general, the substances were found to have

**Table 2**
Minimal inhibition concentrations of target compounds.

| Compounds | Stock Sol. (μg/mL) | Microorganisms and minimal inhibition concentration (MIC, μg/mL) | | | | | | | | |
|---|---|---|---|---|---|---|---|---|---|---|
| | | Gram (−) Bac. | | | Gram (+) Bac. | | | No Gram | Fungi | |
| | | *Ec* | *Yp* | *Pa* | *Sa* | *Ef* | *Bc* | *Ms* | *Ca* | *Sc* |
| **5a** | 17.400 | – | – | – | 435 | 217 | 217 | 217 | 870 | 870 |
| **5b** | 15.600 | 780 | 780 | – | 195 | 195 | 97.5 | 97.5 | 780 | – |
| **5c** | 14.900 | 745 | – | – | 186 | 372 | 372 | 372 | 745 | 745 |
| **5d** | 9.700 | – | – | – | 485 | 485 | 242 | 121 | 485 | 485 |
| **5e** | 26.000 | 1300 | 1300 | – | 650 | 650 | 325 | 325 | 1300 | 1300 |
| **5f** | 800 | – | – | – | – | – | 200 | – | 400 | 400 |
| **5g** | 32.000 | 1600 | 1600 | – | 400 | 1600 | 200 | 200 | 800 | – |
| **5h** | 0.400 | – | – | – | – | – | – | 20 | 10 | – |
| **5i** | 0.500 | – | 25 | – | – | 25 | 25 | 25 | 12.5 | – |
| **5j** | 6810 | – | – | – | – | – | 170 | 85 | 340 | 340 |
| **5k** | 4790 | – | – | – | 239 | 239 | 239 | 60 | 30 | 239 |
| **5l** | 3270 | – | – | – | – | – | 163 | – | – | – |
| **5m** | 1680 | – | – | – | – | – | – | 10,5 | 42 | 84 |
| **5n** | 7010 | – | – | – | – | 355 | 177 | 11 | 177 | 177 |
| **5o** | 7560 | – | – | 378 | 378 | – | 378 | 189 | 378 | – |
| **5p** | 4200 | – | – | – | 210 | – | 26 | 26 | 210 | 210 |
| **5q** | 4690 | – | – | – | 117 | 117 | 58 | 29 | 234 | 234 |
| **5r** | 2190 | – | – | – | – | – | 109 | 55 | 55 | 109 |
| **Amp.** | 10 | 10 | 18 | 128 | 3–5 | 10 | 15 | | | |
| **Strep.** | 10 | | | | | | | 4 | | |
| **Flu** | 5 | | | | | | | | 8 | 8 |

Ec: *Escherichia coli* Yp: *Yersinia pseudotuberculosis* Pa: Pseudomonas aeuriginosa Sa: Staphilococcus aureus Ef: *Enterococcus faecalis* Bc: *Bacillus cereus* Ms.: *Mycobacterium smegmatis* Ca: *Candida albicans* Sc: *Saccharomyces cerevisiae*.
Amp: Ampicillin Strep: Streptomycin Flu: Fluconazole.

antimicrobial activity against at least one microorganism. None of the substances except **5o** had antipseudomal activity and substances **5b, 5e** and **5g** were effective against all microorganism groups (broad spectrum) except *P. aeruginosa*. Substances **5a** and **5d** were effective against other tested microorganisms except Gram-negative bacteria at concentrations of 217–870 and 121–485 μg/mL, respectively. The study found that the most sensitive microorganism to the substances was *M. smegmatis*, which was sensitive to all substances except **5f** and **5l** at concentrations of 10.5–325 μg/mL. Substances **5h** and **5m** were found to be specific and effective against *M. smegmatis* and yeasts at low concentrations (Table 2).

### 2.4. Nuclease activity of the target compounds

Coronaviruses (CoVs) cause respiratory and intestinal infections in animals and humans. The main protease (Mpro), also known as 3CL protease, has a crucial function in the cleavage of polyproteins derived from viral RNA. Potential drug candidates for the treatment of patients with COVID-19 are protease inhibitors that can inhibit viral replication.

An assay kit (BPS Science, 78042-1) was used to determine the inhibitory effect of selected target compounds (test inhibitors) on the SARS-CoV-2 major protease enzyme (3CLpro) and experiments were designed according to the table below (Table 3).

The Untagged 3CL Protease Assay Kit is designed for the detection of 3CL protease activity and is used for screening and profiling in a seamless assay that eliminates time consuming wash steps.

#### 2.4.1. Studies on the genomic double-stranded DNA of E. coli

In the study, bacterial DNA was first tested to evaluate the nuclease activity of the compounds (**5c, 5d, 5g** and **5i**). The nuclease-cutting activities of the compounds (exonuclease activity) were analyzed using purified and amplified *E. coli* gDNA (Table 4).

In the study carried out with genomic double-stranded DNA from *E. coli*, substance **5c** destroyed the gDNA after 30 min, while substance **5i** partially destroyed it and substances **5d** and **5g** were ineffective. Substance **5c** also destroyed the gDNA after 120 min, while substance **5i** partially destroyed it and substances **5d** and **5g** were ineffective. After 240 min, substances **5c** and **5i** partially destroyed the gDNA, while substances **5d** and **5g** were ineffective.

#### 2.4.2. Studies on the RNA of the bee virus (Apis mellifera filamentous virus (AmFV), bp554)

To investigate the nuclease activity of the compounds on the viral genome, the exonuclease activity was tested on the filamentous bee virüs RNA (*AmFV*), which was available in our laboratory before the sensitive *SARS-CoV-2* RNA. *Apis mellifera* filamentous virus (AmFV) is a major virus of honey bees that contains a single double-stranded DNA genome, but its relationship to other parasites and its prevalence are poorly understood. This study, which uses the viral double-stranded DNA genome as a model to observe its activity against double-stranded DNA viral nucleic acids, has the potential to significantly impact our understanding of AmFV. Viral DNA amplified by PCR with specific primers was used for the study. In the study, 20 μl of each strain sample was placed in 3 separate tubes and 5 μl of DNA was added. The first series was kept on a vibrating hot plate at 37° for half an hour and then applied to a 1 % agarose gel and photographed to get an idea of the possible effects of our results (Table 5).

In this careful study, we used cDNA specific for the gene region of honey bee filamentosis virus (*AmFV*) amplified with unique primers. Our results showed that the tested compounds **5c** and **5i** exhibited nuclease activity that potentially cleaved the cDNA from its ends within the first 30 min. This careful approach ensures the validity of our results.

**Table 3**
Experimental design according to data sheet (*BPS Bioscience #78042*).

| Component | Positive control | Test inhibitor | Inhibitor control | Blank |
|---|---|---|---|---|
| 3CL Protease (0.5 ng/μl)[a] | 30 μl | 30 μl | 30 μl | – |
| Assay Buffer (with DTT) | – | – | – | 30 μl |
| GC376 (500 μM) | – | – | 10 μl | – |
| Test Inhibitor | – | 10 μl | – | – |
| Diluent Solution | 10 μl | – | – | 10 μl |
| Total | 40 μl | 40 μl | 40 μl | 40 μl |

[a] 3CL inhibitor GC376 is provided as a technical control for 3CL inhibition.

**Table 4**
Results of substances that interact best with *E. coli* gDNA.

| Compounds | 30 min. | 60 min. | 120 min. | 180 min. | 240 min. |
|---|---|---|---|---|---|
| *E. coli* gDNA | 3+ | 3+ | 3+ smear | 3+ smear | 3+ smear |
| **5c** | 4+ | 2+ | 2+ | 2+ | 2+ |
| **5d** | – | – | – | – | – |
| **5g** | +/− | 1+ | 1+ | +/− | + |
| **5i** | 4+ | 4+ | 4+ | 4+ | 4+ |

#### 2.4.3. Studies on the DNA of the COVID-19 virus

Nucleases obtained by the hydrolysis of the phosphodiester bond in DNA or RNA play a crucial role in pharmacological biotechnology as well as in biological processes involving DNA, such as replication, recombination, molecular cloning, genotyping, and mapping. Literature research has shown that quercetin-3-*O*-glucoside compounds inhibit the main protease enzyme of SARS-CoV-2, proving quercetin-3-*O*-glucoside compounds as natural inhibitors.

The value of the positive control of the enzyme was measured at 12.87 OD and the value of the commercial inhibitory control at 9.978 OD. Using these values, we compared the inhibition values of our synthesized compounds and considered values close to or below the inhibition control values as significant and effective. According to these data, sample **5a** was found to be the most effective against inhibition of the enzyme coronavirus 3CL protease enzyme. In addition samples **5m, 5h, 5i** and **5d,** in that order, showed very strong inhibitory activities (Table 6, Table 7).

In determining the inhibitory activities of the synthesized flavonol-3-*O*-glucoside compounds (compounds **5a–i**) on the SARS-CoV-2 main protease enzyme (3CLpro), data were obtained that overlap with the results of the molecular modeling study. The $IC_{50}$ [μM] values were determined in the context of the kit used. Compared to the reference, the compounds with the lowest inhibitory activity were determined as **5c, 5d, 5g** and **5i**. Some of these compounds were diluted to the extent possible and the most appropriate concentration value for the enzyme substrate was determined. Other compounds could not be diluted due to insufficient kit. In addition, these compounds (**5c, 5d, 5g** and **5i**) were used in nuclease activity studies.

## 3. Conclusion

In summary, we have succeeded in developing and synthesising the flavonol-3-*O*-glycoside derivatives with moderate yields. Their structure was confirmed by spectral analyses (IR, $^{1}$H NMR, $^{13}$C NMR and HRMS). Furthermore, molecular docking studies showed that the developed flavonol-3-*O*-glycoside derivatives of compounds **5a, 5d, 5h, 5i** and **5m**

**Table 5**
Results of substances that interact best with *AmFV*.

| Compounds | 30 min | 120 min | 240 min |
|---|---|---|---|
| *AmFV* cDNA (5 μl) | 4+ | 4+ | 4+ |
| **5c** | 3+ | 1+ | +/− |
| **5d** | 4+ | 1+ | +/− |
| **5 g** | 4+ | 3+ | 3+ |
| **5i** | 1+ | +/− | +/− |

**Table 6**
Results of substances that interact best with *SARS-CoV*-2.

| Compounds | 30 min | 120 min | 240 min |
|---|---|---|---|
| *SARS-CoV*-2 cDNA (5 μl) | 3+ | 3+ | 3+ |
| **5c** | 3+ | 3+ | 3+ |
| **5d** | − | − | − |
| **5g** | +/− | +/− | +/− |
| **5i** | + | + | + |

exhibited a stronger interaction with SARS-CoV-2 3CLpro compared to the reference inhibitor N3. In addition, these target compounds were tested for their antimicrobial activity *in vitro* to determine whether or not the compounds exhibited high antimicrobial activity. The results showed that compounds **5h, 5i, 5m, 5n, 5p** and **5q** exhibited moderate to high antimicrobial activity.

In a study conducted with the COVID-19 OMICRON-BA1 strain, it was observed that out of four chemicals (**5c, 5d, 5g, 5i**), one of them destroyed SARS-CoV-cDNA within 30 min at 37 °C. Compound **5c** had not effect on the covid nucleic acid, while compound **5d** degraded the DNA and exhibited anti-nuclease activity. Compound **5i** was observed to bind the DNA and hold it at the beginning of the well. Compound **5g** destroyed the nucleic acid and fluoresced intensely, especially in the 400 bp band, presumably due to the Br atom in its structure [57].

Finally, we believe that these results confirm the experimental results of the molecular docking studies. *In vitro* studies on anti-SARS-CoV-2 and nuclease activity showed with $IC_{50}$ values that compound **5d** has enormous potential as an anti-COVID-19 agent.

Due to their effective nuclease activity against the COVID-19 OMICRON-BA1 strain, the **5a-i** series synthesized compounds with the flavonol core are believed to be potential alternatives to the drugs currently used to treat COVID-19.

In view of all the results, the preduction of new flavonol-3-*O*-glycoside derivatives and further phase studies (animal studies) can contribute to the development of new and effective COVID-19 drugs.

## 4. Experimental section

### 4.1. Chemistry general methods

All chemicals, reagents and solvents were used as purchased from commercial suppliers and were used without any purification. All sensitive reactions were carried out in dried flasks under nitrogen atmosphere. The progress of all reactions was examined on Merck silica gel 60 $F_{254}$ aluminium TLC (thin layer chromatography, Merck) plates and viewed under UV light (254 nm). Column chromatography was performed with silica gel (230–400 mesh). The melting points of all compounds were measured in degrees (°C) using a Thermo-var instrument with microscope, which may be uncorrected. The IR spectra of the compounds were measured using a Perkin Elmer 1600 Fourier transform infrared spectrophometer (FTIR-ATR) in the range of 4000–400 ($cm^{-1}$) and expressed in wavenumber ($cm^{-1}$). The $^{1}H$ NMR (400 MHz) and $^{13}C$ NMR (100 MHz) spectra were recorded on Bruker Avance III 400 MHz spectrometer, using $CDCl_3$/$CD_3OD$/DMSO-$d_6$/Aceton-$d_6$ as solvent and TMS ($Me_4Si$) as internal standard. Chemical shifts were determined as $\delta$-values (in ppm) and coupling constant in Hertz (Hz), and the multiplicity of signals is described as singlet (s), doublet (d), doublet of the doublet (dd), triplet (t) and multiplet (m), while (br) is used for the broad signal. A high –resolution mass spectrum (HRMS) was recorded with Agilent 1260 Infinity Series LC/Q-TOF.

### 4.2. General procedure for the synthesis of chalcone (*3(a–r)*) derivatives

The procedure was mentioned in our previously published studies [38,58]. The compounds (**3a, 3b, 3c, 3d, 3e, 3f, 3g, 3h, 3i, 3k, 3l, 3o, 3r**) were defined according to the published procedures [46,59–62].

### 4.3. Characterization of compounds (*3j, 3m, 3n, 3p, 3q*)

#### 4.3.1. (2E)-1-(4-fluoro-2-hydroxyphenyl)-3-(2-fluorophenyl)prop-2-en-1-one (*3j*)

Yellow solid; yield: 81 %; Mp: 110–111 °C; IR ($\nu_{max}/cm^{-1}$): 3380 (OH), 3090, 3066, 3042 (aromatic C—H), 1639 (C═O), 1569 (C═C), 1351 (C—F), 1206 (C—O); $^{1}H$ NMR (400 MHz, $CDCl_3$, TMS, $\delta$ ppm): 7.7 (d, $J = 15.4$ Hz, 1H, H-2, A part of the AB system), 7.99 (d, $J = 15.4$ Hz, 1H, H-3, B part of the AB system), 6.69 (m, 1H, H-3′), 6.69 (m, 1H, H-5′), 7.93 (dd, $J = 15.9/7.2$ Hz, 1H, H-6′), 7.22 (t, $J = 7.6$ Hz, 1H, H-3″), 7.6 (t, $J = 7.6$ Hz, 1H, H-4″), 7.15 (m, 1H, H-5″), 7.42 (m, 1H, H-6″), 13.17 (s, 1H, 2′-OH); $^{13}C$ NMR (100 MHz, $CDCl_3$, TMS, $\delta$ ppm): 192.62 (C-1), 124.64 (C-2), 138.62 (C-3), 116.04 (C-1′), 166.27/166.14 (C-2′, $^{3}J_{CF} = 13$ Hz), 105.30/105.06 (C-3′, $^{2}J_{CF} = 24$ Hz), 168.77/166.23 (C-4′, $^{1}J_{CF} = 254$ Hz), 107.36/107.13 (C-5′, $^{2}J_{CF} = 23$ Hz), 132.15/132.04 (C-6′, $^{3}J_{CF} = 11$ Hz), 122.53 (C-1″), 163.17/160.63 (C-2″, $^{1}J_{CF} = 254$ Hz), 116.56/116.34 (C-3″, $^{2}J_{CF} = 22$ Hz), 132.45/132.33 (C-4″, $^{3}J_{CF} = 12$ Hz), 130.32/130.30 (C-5″, $^{3}J_{CF} = 9$ Hz), 122.64/122.55 (C-6″, $^{4}J_{CF} = 2$ Hz); HRMS (ESI-QTOF, positive) *m/z* calcd for $C_{15}H_{10}F_2O_2$ $[M + H]^+$: 261.0649, found: 261.0722.

**Table 7**
*In vitro* inhibitory effects of the target compounds on SARS-CoV-2 3CLpro.

| Compounds | Concentrations (μg/μL) | Inhibition value $IC_{50}$ [μM] | Enzyme control 3CL Protease (0.5 ng/μl) | Inhibitor control Commercial sample GC376 (500 μM) | Blank assay buffer (with DTT) |
|---|---|---|---|---|---|
| **5a** | 0.00416 | 8.42 | 12.87 | 9.98 | 1.794 |
| **5b** | 0.00373 | 27.38 | 12.87 | 9.98 | 1.794 |
| **5c** | 0.00356 | 52.12 | 12.87 | 9.98 | 1.794 |
| **5d** | 0.00223 | 18.06 | 12.87 | 9.98 | 1.794 |
| **5e** | 0.00598 | 26.42 | 12.87 | 9.98 | 1.794 |
| **5f** | 0.000184 | ND | 12.87 | 9.98 | 1.794 |
| **5g** | 0.00669 | 46.65 | 12.87 | 9.98 | 1.794 |
| **5h** | 0.0000836 | 14.85 | 12.87 | 9.98 | 1.794 |
| **5i** | 0.0001045 | 16.11 | 12.87 | 9.98 | 1.794 |
| **5j** | 0.00681 | 61.02 | 12.87 | 9.98 | 1.794 |
| **5k** | 0.00479 | 51.60 | 12.87 | 9.98 | 1.794 |
| **5l** | 0.00327 | 35.14 | 12.87 | 9.98 | 1.794 |
| **5m** | 0.00168 | 14.56 | 12.87 | 9.98 | 1.794 |
| **5n** | 0.00701 | 59.33 | 12.87 | 9.98 | 1.794 |
| **5o** | 0.00756 | 160.76[a] | 12.87 | 9.98 | 1.794 |
| **5p** | 0.00420 | 24.24 | 12.87 | 9.98 | 1.794 |
| **5q** | 0.00469 | 167.21[a] | 12.87 | 9.98 | 1.794 |
| **5r** | 0.00219 | 51.19 | 12.87 | 9.98 | 1.794 |

ND: Not determined.
[a] Due to the decrease in substrate during the study, we were only able to add a reduced amount, resulting in a high value.

*4.3.2. (2E)-1-(4-fluoro-2-hydroxyphenyl)-3-(2-chlorophenyl)prop-2-en-1-one (**3m**)*

Bright yellow solid; yield: 40 %; Mp: 148–149 °C; IR ($\nu_{max}$/cm$^{-1}$): 3104 (OH), 3063 (aromatic C—H), 2922, 2852 (aliphatic C—H), 1638 (C═O), 1563 (C═C), 1350 (C—F), 1204 C-O; $^1$H NMR (400 MHz, $CDCl_3$, TMS, $\delta$ ppm): 7.56 (d, $J$ = 16.0 Hz, 1H, H-2, A part of the AB system), 8.31 (d, $J$ = 16.0 Hz, 1H, H-3, B part of the AB system), 6.69 (m, 1H, H-3′), 6.69 (m, 1H, H-5′), 7.76 (d, $J$ = 8.0 Hz, 1H, H-6′), 7.92 (dd, $J$ = 12.0/4.0 Hz, 1H, H-3″), 7.35 (m, 1H, H-4″), 7.35 (m, 1H, H-5″), 7.47 (d, $J$ = 8.0 Hz, 1H, H-6″), 13.31 (s, 1H, 2'-OH); $^{13}$C NMR (100 MHz, $CDCl_3$, TMS, $\delta$ ppm): 192.36 (C-1), 122.51 (C-2), 141.48 (C-3), 116.97 (C-1′), 166.29/166.20 (C-2′, $^3J_{CF}$ = 9 Hz), 105.40/105.16 (C-3′, $^2J_{CF}$ = 24 Hz), 168.85/166.35 (C-4′, $^1J_{CF}$ = 250 Hz), 107.41/107.18 (C-5′, $^2J_{CF}$ = 23 Hz), 132.16/132.04 (C-6′, $^3J_{CF}$ = 12 Hz), 135.80 (C-1″), 132.82 (C-2″), 130.49 (C-3″), 131.69 (C-4″), 127.19 (C-5″), 127.96 (C-6″); HRMS (ESI-QTOF, positive) $m/z$ calcd for $C_{15}H_{10}ClFO_2$ [M]$^+$: 276.0353, found: 276.2709.

*4.3.3. (2E)-1-(4-fluoro-2-hydroxyphenyl)-3-(3-chlorophenyl)prop-2-en-1-one (**3n**)*

Orange solid; yield: 65 %; Mp: 143–144 °C; IR ($\nu_{max}$/cm$^{-1}$): 3085 (OH), 3016 (aromatic C—H), 2917 (aliphatic C—H), 1643 (C═O), 1566 (C═C), 1352 (C—F), 1206 (C—O); $^1$H NMR (400 MHz, $CDCl_3$, TMS, $\delta$ ppm): 7.56 (d, $J$ = 15.5 Hz, 1H, H-2, A part of the AB system), 7.84 (d, $J$ = 15.5 Hz, 1H, H-3, B part of the AB system), 6.69 (m, 1H, H-3′), 6.69 (m, 1H, H-5′), 7.93 (dd, $J$ = 15.3/6.4 Hz, 1H, H-6′), 7.65 (s, 1H, H-2″), 7.51 (d, $J$ = 7.0 Hz, 1H, H-4″), 7.39 (m, 1H, H-5″), 7.39 (m, 1H, H-6″), 13.11 (s, 1H, 2′-OH); $^{13}$C NMR (100 MHz, $CDCl_3$, TMS, $\delta$ ppm): 192.21 (C-1), 121.60 (C-2), 143.96 (C-3), 116.96 (C-1′), 166.32/166.19 (C-2′, $^3J_{CF}$ = 13 Hz), 105.39/105.15 (C-3′, $^2J_{CF}$ = 24 Hz), 168.87/166.33 (C-4′, $^1J_{CF}$ = 254 Hz), 107.45/107.22 (C-5′, $^2J_{CF}$ = 23 Hz), 132.12/132.00 (C-6′, $^3J_{CF}$ = 12 Hz), 136.21 (C-1″), 128.05 (C-2″), 135.05 (C-3″), 130.36 (C-4″), 130.86 (C-5″), 127.13 (C-6″); HRMS (ESI-QTOF, positive) $m/z$ calcd for $C_{15}H_{10}ClFO_2$ [H]$^+$: 276.0353, found: 276.2786.

*4.3.4. (2E)-1-(4-fluoro-2-hydroxyphenyl)-3-(2-bromophenyl)prop-2-en-1-one (**3p**)*

Bright orange solid; yield: 55 %; Mp: 128–129 °C; IR ($\nu_{max}$/cm$^{-1}$): 3058 (OH), 3023 (aromatic C—H), 2977 (aliphatic C—H), 1638 (C═O), 1565 (C═C), 1348 (C—F), 1204 (C—O); $^1$H NMR (400 MHz, $CDCl_3$, TMS, $\delta$ ppm): 7.50 (d, $J$ = 15.4 Hz, 1H, H-2, A part of the AB system), 8.26 (d, $J$ = 15.4 Hz, 1H, H-3, B part of the AB system), 6.70 (m, 1H, H-3′), 6.70 (m, 1H, H-5′), 7.92 (dd, $J$ = 15.4/6.4 Hz, 1H, H-6′), 7.74 (d, $J$ = 7.8 Hz, 1H, H-3″), 7.28 (t, $J$ = 7.8 Hz,1H, H-4″), 7.38 (t, $J$ = 7.8 Hz, 1H, H-5″), 7.66 (d, $J$ = 7.9 Hz, 1H, H-6″), 13.10 (s, 1H, 2′-OH); $^{13}$C NMR (100 MHz, $CDCl_3$, TMS, $\delta$ ppm): 192.29 (C-1), 122.74 (C-2), 144.03 (C-3), 116.86 (C-1′), 166.30/166.21 (C-2′, $^3J_{CF}$ = 9 Hz), 105.40/105.17 (C-3′, $^2J_{CF}$ = 23 Hz), 168.54/166.35 (C-4′, $^1J_{CF}$ = 219 Hz), 107.41/107.18 (C-5′, $^2J_{CF}$ = 23 Hz), 132.17/132.05 (C-6′, $^3J_{CF}$ = 12 Hz), 134.62 (C-1″), 126.17 (C-2″), 133.75 (C-3″), 131.82 (C-4″), 128.03 (C-5″), 127.81 (C-6″); HRMS (ESI-QTOF, positive) $m/z$ calcd for $C_{15}H_{10}BrFO_2$ [M + H]$^+$: 320.9848, found: 320.9880.

*4.3.5. (2E)-1-(4-fluoro-2-hydroxyphenyl)-3-(3-bromophenyl)prop-2-en-1-one (**3q**)*

Orange solid; yield: 40 %, Mp: 138–139 °C; IR ($\nu_{max}$/cm$^{-1}$): 3084 (OH), 3011 (aromatic C—H), 1642 (C═O), 1572 (C═C), 1347 (C—F), 1203 (C—O); $^1$H NMR (400 MHz, $CDCl_3$, TMS, $\delta$ ppm): 7.55 (m, 1H, H-2, A part of the AB system), 7.83 (d, $J$ = 15.3 Hz, 1H, H-3, B part of the AB system), 6.69 (m, 1H, H-3′), 6.69 (m, 1H, H-5′), 7.93 (m, 1H, H-6′), 7.55 (m, 1H, H-2″), 7.93 (m, 1H, H-4″), 7.55 (m, 1H, H-5″), 7.32 (t, $J$ = 7.8 Hz, 1H, H-6″), 13.10 (s, 1H, 2'-OH); $^{13}$C NMR (100 MHz, $CDCl_3$, TMS, $\delta$ ppm): 192.18 (C-1), 121.18 (C-2), 143.87 (C-3), 116.84 (C-1′), 166.33/166.20 (C-2′, $^3J_{CF}$ = 13 Hz), 105.40/105.16 (C-3′, $^2J_{CF}$ = 24 Hz), 168.88/166.34 (C-4′, $^1J_{CF}$ = 254 Hz), 107.46/107.23 (C-5′, $^2J_{CF}$ = 23 Hz), 132.07/131.95 (C-6′, $^3J_{CF}$ = 12 Hz), 136.43 (C-1″), 133.80 (C-2″), 123.21 (C-3″), 127.59 (C-4″), 130.92 (C-5″), 130.63 (C-6″); HRMS (ESI-QTOF, positive) $m/z$ calcd for $C_{15}H_{10}BrFO_2$ [M + H]$^+$: 319.9848, found: 320.2952.

*4.4. General procedure for the synthesis of flavonol (**4(a–r)**) derivatives*

2′-Hydroxychalcone derivatives (**3(a–r)**) (1 eq), $Na_2CO_3$ (1 eq) and hydrogen peroxide (35 %, 1 mL) in methanol (30 mL) was stirred vigorously on ice for 1 h and then maintained room temperature. After completion of the reaction, which was monitored by TLC, hydrochloric acid (HCl, 10 %) was added to the reaction mixture to neutralize it, resulting in a precipitate. These precipitates were filtered under reduced pressure, washed with water and used for future purification (column chromatography or crystallization) to obtain pure flavonol (**4(a–r)**). The purity of flavonol compounds is ≥45 %. The compounds (**4a, 4b, 4c, 4d, 4e, 4f, 4g, 4h, 4i, 4o**) and the details of their structural characterization have been described previously [46,63–65].

*4.5. Characterization of compounds (**4j, 4k, 4l, 4m, 4n, 4p, 4q, 4r**)*

*4.5.1. 2-(2-fluorophenyl)-7-fluoro-3-hydroxy-4H-chromen-4-one (**4j**)*

Bright yellow solid; yield: 48 %; Mp:156–157 °C; IR ($\nu_{max}$/cm$^{-1}$): 3299 (OH), 3080 (aromatic C—H), 1611 (C═O), 1459 (C═C), 1205 (C—F), 1155 (C—O); $^1$H NMR (400 MHz, Aceton-$d_6$, TMS, $\delta$ ppm): 8.26 (dd, $J$ = 15.4/5.0 Hz, 1H, H-5), 7.40 (m, 1H, H-6), 7.40 (m, 1H, H-8), 7.40 (m, 1H, H-3′), 7.63 (m, 1H, H-4′), 7.40 (m, 1H, H-5′), 7.87 (t, $J$ = 8.5 Hz,1H, H-6′); $^{13}$C NMR (100 MHz, Aceton-$d_6$, TMS, $\delta$ ppm): 142.99 (C-2), 139.70 (C-3), 172.35 (C-4), 128.04/127.93 (C-5, $^3J_{CF}$ = 11 Hz), 113.60/113.37 (C-6, $^2J_{CF}$ = 23 Hz), 166.79/164.29 (C-7, $^1J_{CF}$ = 250 Hz), 104.85/104.60 (C-8, $^2J_{CF}$ = 25 Hz), 156.78/156.66 (C-9, $^3J_{CF}$ = 12 Hz), 118.94 (C-10), 117.29 (C-1′), 161.04/158.55 (C-2′, $^1J_{CF}$ = 249 Hz), 116.26/116.05 (C-3′, $^2J_{CF}$ = 21 Hz), 132.51/132.43 (C-4′, $^3J_{CF}$ = 8 Hz), 124.30/124.27 (C-5′, $^4J_{CF}$ = 3 Hz), 131.22 (C-6′); HRMS (ESI-QTOF, positive) $m/z$ calcd for $C_{15}H_8F_2O_3$ [M + H]$^+$: 275.219, found: 275.0473.

*4.5.2. 2-(3-fluorophenyl)-7-fluoro-3-hydroxy-4H-chromen-4-one (**4k**)*

Yellow solid; yield: 45 %; Mp: 200–201 °C; IR ($\nu_{max}$/cm$^{-1}$): 3315 (OH), 3080 (aromatic C—H), 2923 (aliphatic C—H), 1602 (C═O), 1578 (C═C), 1218 (C—F), 1182 (C—O); $^1$H NMR (400 MHz, $CDCl_3$/$CD_3OD$, TMS, $\delta$ ppm): 8.19 (m, 1H, H-5), 6.88 (m, 1H, H-6), 7.07 (d, $J$ = 9.5 Hz, 1H, H-8), 7.98 (dd, $J$ = 15.4/6.5 Hz, 1H, H-2′), 6.88 (m, 1H, H-4′), 7.30 (m, 1H, H-5′), 8.07 (d, $J$ = 8.1 Hz,1H, H-6′); $^{13}$C NMR (100 MHz, $CDCl_3$/$CD_3OD$, TMS, $\delta$ ppm): 145.38 (C-2), 135.96 (C-3), 179.50 (C-4), 126.94/126.84 (C-5, $^3J_{CF}$ = 10 Hz), 112.86/112.61 (C-6, $^2J_{CF}$ = 25 Hz), 165.59/163.33 (C-7, $^1J_{CF}$ = 226 Hz), 103.56/103.31 (C-8, $^2J_{CF}$ = 25 Hz), 121.34 (C-9), 118.42 (C-10), 135.82 (C-1′), 111.75/111.51 (C-2′, $^2J_{CF}$ = 24 Hz), 162.87/160.95 (C-3′, $^1J_{CF}$ = 192 Hz), 113.67/113.46 (C-4′, $^2J_{CF}$ = 21 Hz),128.87/128.78 (C-5′, $^3J_{CF}$ = 9 Hz), 121.30 (C-6′); HRMS (ESI-QTOF, positive) $m/z$ calcd for $C_{15}H_8F_2O_3$ [M + H]$^+$: 275.219, found: 275.2776.

*4.5.3. 2-(4-fluorophenyl)-7-fluoro-3-hydroxy-4H-chromen-4-one (**4l**)*

Yellow solid; yield: 68 %; Mp:193–194 °C; IR ($\nu_{max}$/cm$^{-1}$): 3256 (OH), 3085 (aromatic C—H), 2925 (aliphatic C—H), 1603 (C═O), 1574 (C═C), 1230 (C—F), 1159 (C—O); $^1$H NMR (400 MHz, $CDCl_3$, TMS, $\delta$ ppm): 8.25 (m, 1H, H-5), 7.22 (m, 1H, H-6), 7.22 (m, 1H, H-8), 8.25 (m, 2H, H-2′/6′), 7.22 (m, 2H, H-3′/5′); $^{13}$C NMR (100 MHz, $CDCl_3$, TMS, $\delta$ ppm): 144.56 (C-2), 138.04 (C-3), 172.75 (C-4), 128.13/128.02 (C-5, $^3J_{CF}$ = 11 Hz), 114.13/113.90 (C-6, $^2J_{CF}$ = 23 Hz), 167.09/164.92 (C-7, $^1J_{CF}$ = 217 Hz), 104.86/104.61 (C-8,$^2J_{CF}$ = 25 Hz), 156.38/156.24 (C-9, $^3J_{CF}$ = 14 Hz), 117.56 (C-10), 126.93 (C-1′), 129.95/129.87 (C-2′/6′, $^3J_{CF}$ = 8 Hz), 116.00/115.78(C-3′/5′, $^2J_{CF}$ = 22 Hz), 164.54/162.41 (C-4′, $^1J_{CF}$ = 213 Hz); HRMS (ESI-QTOF, positive) $m/z$ calcd for $C_{15}H_8F_2O_3$ [M + H]$^+$: 275.219, found: 275.2776.

*4.5.4. 2-(2-chlorophenyl)-7-fluoro-3-hydroxy-4H-chromen-4-one (**4m**)*

Light orange solid; yield: 47 %; Mp: 163–164 °C; IR ($\nu_{max}$/cm$^{-1}$):

3300 (OH), 3099 (aromatic C—H), 2924 (aliphatic C—H), 1613 (C═O), 1407 (C═C), 1210 (C—F), 1158 C—O; $^{1}$H NMR (400 MHz, Aseton-$d_6$, TMS, $\delta$ ppm): 8.30 (dd, $J$ = 15.8/6.4 Hz, 1H, H-5), 7.20 (m, 1H, H-6), 7.20 (m, 1H, H-8), 7.55 (d, $J$ = 8.2 Hz, 1H, H-3′), 7.43 (m, 1H, H-4′), 7.43 (m, 1H, H-5′), 7.65 (d, $J$ = 8.5 Hz,1H, H-6′); $^{13}$C NMR (100 MHz, Aseton-$d_6$, TMS, $\delta$ ppm): 145.69 (C-2), 138.89 (C-3), 172.88 (C-4), 128.24/128.13 (C-5, $^{3}J_{CF}$ = 11 Hz), 114.22/113.98 (C-6, $^{2}J_{CF}$ = 24 Hz), 167.10/164.56 (C-7, $^{1}J_{CF}$ = 254 Hz), 105.05/104.80 (C-8, $^{2}J_{CF}$ = 25 Hz), 156.94/156.80 (C-9, $^{3}J_{CF}$ = 14 Hz), 118.23 (C-10), 129.22 (C-1′), 133.86 (C-2′), 131.58 (C-3′), 131.75 (C-4′), 130.43 (C-5′), 126.81 (C-6′); HRMS (ESI-QTOF, positive) $m/z$ calcd for $C_{15}H_8ClFO_3$ [M + H]$^+$: 291.0146, found: 291.0185.

#### 4.5.5. 2-(3-chlorophenyl)-7-fluoro-3-hydroxy-4H-chromen-4-one (4n)

Orange solid; yield: 53 %; Mp: 162–163 °C; IR ($\nu_{max}$/cm$^{-1}$): 3311 (OH), 3087 (aromatic C—H), 2924 (aliphatic C—H), 1607 (C═O), 1446 (C═C), 1204 (C—F), 1047 (C—O); $^{1}$H NMR (400 MHz, Aseton-$d_6$, TMS, $\delta$ ppm):8.14 (d, $J$ = 7.5 Hz, 1H, H-5), 7.19 (t, $J$ = 8.6 Hz, 1H, H-6), 7.47 (m, 1H, H-8), 8.20 (bs, 1H, H-2′), 7.47 (m, 1H, H-4′), 7.47 (m, 1H, H-5′), 8.10 (dd, $J$ = 15.3/5.6 Hz,1H, H-6′), 8.45 (s, 1H, 3-OH); $^{13}$C NMR (100 MHZ, Aseton-$d_6$, TMS, $\delta$ ppm): 143.32 (C-2), 139.47 (C-3), 172.51 (C-4), 127.89/127.78 (C-5, $^{3}J_{CF}$ = 11 Hz), 113.71/113.48 (C-6, $^{2}J_{CF}$ = 23 Hz), 167.03/164.49 (C-7, $^{1}J_{CF}$ = 254 Hz), 105.01/104.76 (C-8, $^{2}J_{CF}$ = 25 Hz), 156.39/156.25 (C-9, $^{3}J_{CF}$ = 14 Hz), 118.12 (C-10), 133.28 (C-1′), 127.05 (C-2′), 134.16 (C-3′), 129.71 (C-4′),130.20 (C-5′), 125.95 (C-6′); HRMS (ESI-QTOF, positive) $m/z$ calcd for $C_{15}H_8ClFO_3$ [M + H]$^+$: 291.0146, found: 291.0191.

#### 4.5.6. 2-(2-bromophenyl)-7-fluoro-3-hydroxy-4H-chromen-4-one (4p)

Bright yellow solid; yield: 62 %; Mp: 187–188 °C; IR ($\nu_{max}$/cm$^{-1}$): 3264 (OH), 3095 (aromatic C—H), 2812 (aliphatic C—H), 1607 (C═O), 1403 (C═C), 1156 (C—F), 1117 (C—O); $^{1}$H NMR (400 MHz, Aseton-$d_6$/$CDCl_3$/$CD_3OD$, TMS, $\delta$ ppm): 7.99 (dd, $J$ = 15.2/6.2 Hz, 1H, H-5), 6.94 (m, 1H, H-6), 7.11 (m, 1H, H-8), 7.46 (d, $J$ = 8.0 Hz, 1H, H-3′), 6.94 (m, 1H, H-4′), 7.20 (t, $J$ = 7.4 Hz, 1H, H-5′), 7.35 (d, $J$ = 7.7 Hz,1H, H-6′); $^{13}$C NMR (100 MHz, Aseton-$d_6$/$CDCl_3$/$CD_3OD$, TMS, $\delta$ ppm): 147.19 (C-2), 138.78 (C-3), 172.88 (C-4), 127.75/127.62 (C-5, $^{3}J_{CF}$ = 13 Hz), 113.69/113.46 (C-6, $^{2}J_{CF}$ = 23 Hz), 166.71/164.13 (C-7, $^{1}J_{CF}$ = 258 Hz), 104.50/104.32 (C-8, $^{2}J_{CF}$ = 18 Hz), 156.40/156.30 (C-9, $^{3}J_{CF}$ = 10 Hz), 118.65 (C-10), 131.41 (C-1′), 122.71 (C-2′), 132.97 (C-3′), 131.54 (C-4′), 131.44 (C-5′), 127.14 (C-6′); HRMS (ESI-QTOF, positive) $m/z$ calcd for $C_{15}H_8BrFO_3$ [M-H]$^+$: 332.9641, found: 332.3146.

#### 4.5.7. 2-(3-bromophenyl)-7-fluoro-3-hydroxy-4H-chromen-4-one (4q)

Pale yellow solid; yield: 51 %; Mp: 169–170 °C; IR ($\nu_{max}$/cm$^{-1}$): 3261 (OH), 3095 (aromatic C—H), 1601(C═O), 1455 (C═C), 1210 (C—F), 1163 (C—O); $^{1}$H NMR (400 MHz, $CDCl_3$, TMS, $\delta$ ppm): 8.25 (dd, $J$ = 15.1/6.2 Hz, 1H, H-5), 7.17 (m, 1H, H-6), 7.40 (t, $J$ = 8.0 Hz, 1H, H-8), 8.34 (bs, 1H, H-2′), 7.60 (d, $J$ = 7.9 Hz 1H, H-4′), 7.28 (d, $J$ = 7.2 Hz, 1H, H-5′), 8.18 (d, $J$ = 6.6 Hz,1H, H-6′); $^{13}$C NMR (100 MHZ, $CDCl_3$, TMS, $\delta$ ppm): 143.45 (C-2), 138.77 (C-3), 172.77 (C-4), 128.18/128.07 (C-5, $^{3}J_{CF}$ = 11 Hz), 114.26/114.02 (C-6, $^{2}J_{CF}$ = 24 Hz), 167.18/164.68 (C-7, $^{1}J_{CF}$ = 250 Hz), 104.95/104.70 (C-8, $^{2}J_{CF}$ = 25 Hz), 156.42/156.32 (C-9, $^{3}J_{CF}$ = 10 Hz), 117.49 (C-10), 122.89 (C-1′), 133.14 (C-2′), 132.54 (C-3′), 130.21 (C-4′),130.18 (C-5′), 126.24 (C-6′); HRMS (ESI-QTOF, positive) $m/z$ calcd for $C_{15}H_8BrFO_3$ [M + H]$^+$: 334.9641, found: 334.9667.

#### 4.5.8. 2-(4-bromophenyl)-7-fluoro-3-hydroxy-4H-chromen-4-one (4r)

Yellow solid; yield: 46 %; Mp: 186–187 °C; IR ($\nu_{max}$/cm$^{-1}$): 3241 (OH), 3076 (aromatic C—H), 1598 (C═O), 1455 (C═C), 1210 (C—F), 1162 (C—O); $^{1}$H NMR (400 MHz, Aseton-$d_6$, TMS, $\delta$ ppm): 8.26 (m, 1H, H-5), 7.33 (t, $J$ = 6.8 Hz, 1H, H-6), 7.60 (d, $J$ = 6.6 Hz, 1H, H-8), 8.26 (m, 2H, H-2′/6′), 7.78 (d, $J$ = 8.4 Hz, 2H, H-3′/5′), 8.54 (s, 1H, 3-OH); $^{13}$C NMR (100 MHz, Aseton-$d_6$, TMS, $\delta$ ppm): 143.81 (C-2), 139.24 (C-3), 172.41 (C-4), 127.89/127.78 (C-5, $^{3}J_{CF}$ = 11 Hz), 113.64/113.41 (C-6, $^{2}J_{CF}$ = 23 Hz), 166.92/164.45 (C-7, $^{4}J_{CF}$ = 247 Hz), 104.91/104.65 (C-8, $^{2}J_{CF}$ = 26 Hz), 156.23 (C-9), 118.25 (C-10), 130.47 (C-1′), 129.34 (C-2′/6′), 131.71 (C-3′/5′), 123.69 (C-4′); HRMS (ESI-QTOF, positive) $m/z$ calcd for $C_{15}H_8BrFO_3$ [M + H]$^+$: 334.9641, found: 334.9656.

### 4.6. General procedure for the synthesis of flavonol-3-O-glycosides (5 (a–r)) derivatives

The synthesis procedures for the flavonol-3-*O*-glycosides (**5(a–r)**) were defined based on previous work [42,45,53].

### 4.7. Characterization of compounds (5(a–r))

#### 4.7.1. 2-(2-fluorophenyl)-3-O-β-D-glucopyranosyl-4H-chromen-4-one (5a)

White powder; yield: 20 %; Mp: 141–142 °C; IR ($\nu_{max}$/cm$^{-1}$): 3322 (OH), 2968 (glucosidic C—H), 2922 (aliphatic C—H), 1613 (C═O), 1466 (C═C), 1205 (C—F), 1056 (C—O), 908 (β-configuration of anomeric carbon); $^{1}$H NMR (400 MHz, $CD_3OD$, TMS, $\delta$ ppm): 8.24 (d, 1H, H-5, $J$ = 7.4 Hz), 7.57 (m, 3H, H-6/7/8), 7.32 (m, 2H, H-3′/5′), 7.83 (t, 1H, H-4′, $J$ = 7.0 Hz), 7.90 (t, 1H, H-6′, $J$ = 7.4 Hz), 5.19 (d, 1H, β-anomeric proton, $J$ = 7.2 Hz), 3.06–3.76 (m, 6H, glucosidic C—H); $^{13}$C NMR (100 MHz, $CD_3OD$, TMS, $\delta$ ppm): 155.41 (C-2), 137.91 (C-3), 174.95 (C-4), 125.17 (C-5), 123.52 (C-6), 134.31 (C-7), 118.14 (C-8), 155.78 (C-9), 123.72 (C-10), 118.98/118.84 (C-1′, $^{2}J$ = 13.8 Hz), 161.30/158.80 (C-2′, $^{1}J$ = 250.4 Hz), 115.61/115.39 (C-3′, $^{2}J$ = 21.1 Hz), 132.60/132.51 (C-4′, $^{3}J$ = 8.7 Hz), 123.56/123.52 (C-5′, $^{4}J$ = 3.6 Hz), 131.98/131.95 (C-6′, $^{3}J$ = 2.1 Hz), 102.17 (β-anomeric carbon), 74.07 (Glu/C-2), 76.26 (Glu/C-3), 69.72 (Glu/C-4), 76.89 (Glu/C-5), 61.07 (Glu/C-6); HRMS (ESI-QTOF, positive) $m/z$ calcd for $C_{21}H_{19}FO_8$ [M + H]$^+$: 419.1064, found: 419.1134.

#### 4.7.2. 2-(3-fluorophenyl)-3-O-β-D-glucopyranosyl-4H-chromen-4-one (5b)

Pale yellow powder; yield: 23 %; Mp: 135–136 °C; IR ($\nu_{max}$/cm$^{-1}$): 3318 (OH), 2960 (glucosidic C—H), 2921 (aliphatic C—H), 1604 (C═O), 1480 (C═C), 1210 (C—F), 1054 (C—O), 887 (β-configuration of anomeric carbon); $^{1}$H NMR (400 MHz, $CD_3OD$, TMS, $\delta$ ppm): 8.20 (d, 1H, H-5, $J$ = 7.4 Hz), 7.55 (m, 2H, H-6/5′), 7.83 (t, 1H, $J$ = 7.0 Hz), 7.71 (d, 1H, $J$ = 8.0 Hz), 8.02 (m, 2H, H-2′/6′), 7.29 (m, 1H, H-4′), 5.45 (d, 1H, β-anomeric proton, $J$ = 7.7 Hz), 3.15–3.80 (m, 6H, glucosidic C—H); $^{13}$C NMR (100 MHz, $CD_3OD$, TMS, $\delta$ ppm): 155.55 (C-2), 137.13 (C-3), 175.13 (C-4), 129.16 (C-5), 125.02/124.97 (C-6, $^{4}J$ = 4.8 Hz), 134.19 (C-7), 118.05 (C-8), 155.41 (C-9), 123.49 (C-10), 132.85/132.77 (C-1′, $^{3}J$ = 7.7 Hz), 116.08/115.86 (C-2′, $^{2}J$ = 22.4 Hz), 163.54/161.12 (C-3′, $^{1}J$ = 241.6 Hz), 117.39/117.16 (C-4′, $^{2}J$ = 22.4 Hz), 129.83/129.70 (C-5′, $^{3}J$ = 12.8 Hz), 124.96/124.91 (C-6′, $^{4}J$ = 2.8 Hz), 101.90 (β-anomeric carbon), 74.23 (Glu/C-2), 75.58 (Glu/C-3), 70.02 (Glu/C-4), 77.16 (Glu/C-5), 61.20 (Glu/C-6); HRMS (ESI-QTOF, positive) $m/z$ calcd for $C_{21}H_{19}FO_8$ [M + H]$^+$: 419.1064, found: 419.1137.

#### 4.7.3. 2-(4-fluorophenyl)-3-O-β-D-glucopyranosyl-4H-chromen-4-one (5c) [45]

Yellow powder; yield: 26 %; Mp: 172–173 °C; IR ($\nu_{max}$/cm$^{-1}$): 3295 (OH), 2965 (glucosidic C—H), 2922 (aliphatic C—H), 1600 (C═O), 1469 (C═C), 1204 (C—F), 1047 (C—O), 904 (β-configuration of anomeric carbon); $^{1}$H NMR (400 MHz, $CD_3OD$, TMS, $\delta$ ppm): 8.21 (d, 1H, H-5, $J$ = 7.6 Hz), 7.51 (t, 1H, H-6, $J$ = 7.4 Hz), 7.83 (t, 1H, H-7, $J$ = 7.4 Hz), 7.70 (d, 1H, H-8, $J$ = 7.7 Hz), 8.28 (t, 2H, H-2′/6′, $J$ = 7.2 Hz), 7.28 (t, 2H, H-3′/5′, $J$ = 8.8 Hz), 5.38 (d, 1H, β-anomeric proton, $J$ = 7.3 Hz), 3.10–3.80 (m, 6H, glucosidic C—H); $^{13}$C NMR (100 MHz, $CD_3OD$, TMS, $\delta$ ppm): 156.77 (C-2), 136.85 (C-3), 175.99 (C-4), 124.96 (C-5), 124.98 (C-6), 134.08 (C-7), 117.98 (C-8), 155.43 (C-9), 123.48 (C-10), 127.05/127.01 (C-1′, $^{4}J$ = 3.3 Hz), 131.73/131.62 (C-2′/6′, $^{3}J$ = 10.5 Hz), 114.96/114.72 (C-3′/5′, $^{2}J$ = 23.7 Hz), 165.43/162.94 (C-4′, $^{1}J$ = 249.3 Hz), 102.24 (β-anomeric carbon), 74.30 (Glu/C-2), 76.68 (Glu/C-3), 69.92 (Glu/C-4), 77.13 (Glu/C-5), 61.59 (Glu/C-6); HRMS (ESI-QTOF, positive) $m/z$ calcd for $C_{21}H_{19}FO_8$ [M + H]$^+$: 419.1064, found: 419.1134.

#### 4.7.4. 2-(2-chlorophenyl)-3-O-β-D-glucopyranosyl-4H-chromen-4-one (5d)

Light yellow oil; yield: 21 %; IR ($\nu_{max}$/cm$^{-1}$): 3325 (OH), 2947 (glucosidic C—H), 2846 (aliphatic C—H), 1643 (C═O), 1427 (C═C), 1118 (C—F), 1018 (C—O), 890 (β-configuration of anomeric carbon); $^1$H NMR (400 MHz, $CD_3OD$, TMS, $\delta$ ppm): 8.24 (d, 1H, H-5, $J$ = 8.0 Hz), 7.56 (m, 4H, H-6/8/4′/5′), 7.84 (m, 2H, H-7/3′), 8.07 (s, 1H, H-6′), 5.15 (d, 1H, β-anomeric proton, $J$ = 7.8 Hz), 3.04–3.88 (m, 6H, glucosidic C—H); $^{13}$C NMR (100 MHz, $CD_3OD$, TMS, $\delta$ ppm): 157.64 (C-2), 137.97 (C-3), 175.16 (C-4), 125.15 (C-5), 125.10 (C-6), 134.29 (C-7), 118.12 (C-8), 155.75 (C-9), 129.87 (C-10), 123.78 (C-1′), 133.22 (C-2′), 131.64 (C-3′), 132.41 (C-4′), 129.28 (C-5′), 126.39 (C-6′), 102.55 (β-anomeric carbon), 74.03 (Glu/C-2), 76.46 (Glu/C-3), 69.78 (Glu/C-4), 76.89 (Glu/C-5), 61.10 (Glu/C-6); HRMS (ESI-QTOF, positive) $m/z$ calcd for $C_{21}H_{19}ClO_8$ [M + H]$^+$: 435.0768, found: 435.0839.

#### 4.7.5. 2-(3-chlorophenyl)-3-O-β-D-glucopyranosyl-4H-chromen-4-one (5e)

White solid; yield: 31 %; Mp: 100–101 °C; IR ($\nu_{max}$/cm$^{-1}$): 3301 (OH), 2940 (glucosidic C—H), 2920 (aliphatic C—H), 1617 (C═O), 1469 (C═C), 1206 (C—F), 1060 (C—O), 887 (β-configuration of anomeric carbon); $^1$H NMR (400 MHz, $CD_3OD$, TMS, $\delta$ ppm): 8.19 (d, 1H, H-5, $J$ = 7.8 Hz), 7.52 (m, 3H, H-6/8/5′), 7.69 (d, 1H, H-7, $J$ = 8.0 Hz), 8.24 (s, 1H, H-2′), 7.82 (t, 1H, H-4′, $J$ = 7.4 Hz), 8.10 (s, 1H, H-6′), 5.46 (d, 1H, β-anomeric proton, $J$ = 7.2 Hz), 3.15–9.94 (m, 6H, glucosidic C—H); $^{13}$C NMR (100 MHz, $CD_3OD$, TMS, $\delta$ ppm): 155.96 (C-2), 133.78 (C-3), 175.09 (C-4), 129.00 (C-5), 125.02 (C-6), 134.18 (C-7), 118.06 (C-8), 155.43 (C-9), 123.51 (C-10), 132.55 (C-1′), 129.15 (C-2′), 137.12 (C-3′), 129.49 (C-4′), 130.38 (C-5′), 127.34 (C-6′), 101.86 (β-anomeric carbon), 74.32 (Glu/C-2), 75.54 (Glu/C-3), 70.06 (Glu/C-4), 77.23 (Glu/C-5), 61.13 (Glu/C-6); HRMS (ESI-QTOF, positive) $m/z$ calcd for $C_{21}H_{19}ClO_8$ [M + H]$^+$: 435.0768, found: 435.0836.

#### 4.7.6. 2-(4-chlorophenyl)-3-O-β-D-glucopyranosyl-4H-chromen-4-one (5f) [45]

White solid; yield: 23 %; Mp: 136–137 °C; IR ($\nu_{max}$/cm$^{-1}$): 3317 (OH), 2939 (glucosidic C—H), 2831 (aliphatic C—H), 1611 (C═O), 1427 (C═C), 1203 (C—O), 1111 (C—F), 1018 (C—O), 898 (β-configuration of anomeric carbon); $^1$H NMR (400 MHz, $CD_3OD$, TMS, $\delta$ ppm): 7.83 (t, 1H, H-5, $J$ = 7.8 Hz), 7.57 (m, 4H, H-6/8/3′/5′), 7.72 (m, 1H, H-7), 8.22 (d, 2H, H-2′/6′, $J$ = 7.8 Hz), 5.41 (d, 1H, β-anomeric proton, $J$ = 7.2 Hz), 3.04–3.87 (m, 6H, glucosidic C—H); $^{13}$C NMR (100 MHz, $CD_3OD$, TMS, $\delta$ ppm): 155.42 (C-2), 133.84 (C-3), 175.09 (C-4), 127.91 (C-5), 124.95 (C-6), 134.06 (C-7), 117.94 (C-8), 151.12 (C-9), 123.47 (C-10), 127.27 (C-1′), 132.50 (C-2′/6′), 130.73 (C-3′/5′), 136.66 (C-4′), 101.92 (β-anomeric carbon), 74.27 (Glu/C-2), 76.51 (Glu/C-3), 69.70 (Glu/C-4), 77.24 (Glu/C-5), 61.12 (Glu/C-6); HRMS (ESI-QTOF, positive) $m/z$ calcd for $C_{21}H_{19}ClO_8$ [M + H]$^+$: 435.0768, found: 435.0840.

#### 4.7.7. 2-(2-bromophenyl)-3-O-β-D-glucopyranosyl-4H-chromen-4-one (5g)

Yellow oil; yield: 24 %; IR ($\nu_{max}$/cm$^{-1}$): 3332 (OH), 2939 (glucosidic C—H), 2839 (aliphatic C—H), 1627 (C═O), 1442 (C═C), 1226 (C—F), 1026 (C—O), 894 (β-configuration of anomeric carbon); $^1$H NMR (400 MHz, $CD_3OD$, TMS, $\delta$ ppm): 8.25 (d, 1H, H-5, $J$ = 8.0 Hz), 7.48 (m, 3H, H-6/4′/5′), 7.75 (d, 1H, H-7, $J$ = 7.8 Hz), 7.62 (d, 1H, H-8, $J$ = 8.0 Hz), 7.82 (m, 2H, H-3′/6′), 5.14 (d, 1H, β-anomeric proton, $J$ = 7.8 Hz), 3.09–3.96 (m, 6H, glucosidic C—H); $^{13}$C NMR (100 MHz, $CD_3OD$, TMS, $\delta$ ppm): 158.69 (C-2), 137.82 (C-3), 175.26 (C-4), 125.18 (C-5), 125.09 (C-6), 134.33 (C-7), 118.16 (C-8), 155.71 (C-9), 131.86 (C-10), 123.80 (C-1′), 122.34 (C-2′), 132.55 (C-3′), 132.46 (C-4′), 131.74 (C-5′), 126.94 (C-6′), 102.65 (β-anomeric carbon), 73.99 (Glu/C-2), 76.46 (Glu/C-3), 69.73 (Glu/C-4), 76.89 (Glu/C-5), 61.13 (Glu/C-6); HRMS (ESI-QTOF, positive) $m/z$ calcd for $C_{21}H_{19}BrO_8$ [M + H]$^+$: 479.0263, found: 479.0327.

#### 4.7.8. 2-(3-bromophenyl)-3-O-β-D-glucopyranosyl-4H-chromen-4-one (5h)

Yellow solid; yield: 25 %; Mp: 132–133 °C; IR ($\nu_{max}$/cm$^{-1}$): 3272 (OH), 2958 (glucosidic C—H), 2923 (aliphatic C—H), 1615 (C═O), 1470 (C═C), 1102 (C—F), 1059 (C—O), 887 (β-configuration of anomeric carbon); $^1$H NMR (400 MHz, $CD_3OD$, TMS, $\delta$ ppm): 8.17 (m, 2H, H-5/6′), 7.47 (m, 2H, H-6/5′), 7.81 (t, 1H, H-7, $J$ = 7.8 Hz), 7.68 (d, 2H, H-8/4′, $J$ = 8.0 Hz), 8.43 (s, 1H, H-2′), 5.48 (d, 1H, β-anomeric proton, $J$ = 7.8 Hz), 3.16–3.84 (m, 6H, glucosidic C—H); $^{13}$C NMR (100 MHz, $CD_3OD$, TMS, $\delta$ ppm): 155.61 (C-2), 137.08 (C-3), 175.05 (C-4), 129.16 (C-5), 125.01 (C-6), 134.16 (C-7), 118.05 (C-8), 155.40 (C-9), 121.63 (C-10), 132.73 (C-1′), 133.33 (C-2′), 123.54 (C-3′), 131.92 (C-4′), 129.69 (C-5′), 127.70 (C-6′), 101.80 (β-anomeric carbon), 74.34 (Glu/C-2), 76.53 (Glu/C-3), 70.09 (Glu/C-4), 77.24 (Glu/C-5), 61.34 (Glu/C-6); HRMS (ESI-QTOF, positive) $m/z$ calcd for $C_{21}H_{19}BrO_8$ [M + H]$^+$: 479.0263, found: 479.0327.

#### 4.7.9. 2-(4-bromophenyl)-3-O-β-D-glucopyranosyl-4H-chromen-4-one (5i)

White oil; yield: 21 %; IR ($\nu_{max}$/cm$^{-1}$): 3318 (OH), 2948 (glucosidic C—H), 2920 (aliphatic C—H), 1616 (C═O), 1471 (C═C), 1205 (C—F), 1023 (C—O), 859 (β-configuration of anomeric carbon); $^1$H NMR (400 MHz, $CD_3OD$, TMS, $\delta$ ppm): 8.21 (d, 1H, H-5, $J$ = 8.0 Hz), 7.52 (t, 1H, H-6, $J$ = 8.0 Hz), 7.85 (t, 1H, H-7, $J$ = 7.8 Hz), 7.7 (m, 3H, H-8/3′/5′), 8.10 (m, 2H, H-2′/6′), 5.30 (d, 1H, β-anomeric proton, $J$ = 7.7 Hz), 3.21–4.30 (m, 6H, glucosidic C—H); $^{13}$C NMR (100 MHz, $CD_3OD$, TMS, $\delta$ ppm): 156.82 (C-2), 136.99 (C-3), 174.97 (C-4), 125.12 (C-5), 124.98 (C-6), 134.27 (C-7), 118.08 (C-8), 155.44 (C-9), 123.37 (C-10), 129.77 (C-1′), 130.80 (C-2′/6′), 131.07 (C-3′/5′), 125.05 (C-4′), 102.35 (β-anomeric carbon), 74.21 (Glu/C-2), 74.26 (Glu/C-3), 69.80 (Glu/C-4), 76.41 (Glu/C-5), 62.57 (Glu/C-6); HRMS (ESI-QTOF, positive) $m/z$ calcd for $C_{21}H_{19}BrO_8$ [M + H]$^+$: 479.0263, found: 479.0325.

#### 4.7.10. 2-(2-fluorophenyl)-7-fluoro-3-O-β-D-glucopyranosyl-4H-chromen-4-one (5j)

Bright yellow powder; yield: 30 %; Mp: 180–181 °C; IR ($\nu_{max}$/cm$^{-1}$): 3348 (OH), 2950 (glucosidic C—H), 2925 (aliphatic C—H), 1619 (C═O), 1445 (C═C), 1201 (C—F), 1055 (C—O), 852 (β-configuration of anomeric carbon); $^1$H NMR (400 MHz, Aseton-$d_6$, TMS, $\delta$ ppm): 8.15 (dd, 1H, H-5, $J$ = 15.2, 6.2 Hz), 7.25 (m, 3H, H-6/3′/4′), 7.51 (m, 1H, H-8), 7.36 (d, 1H, H-5′, $J$ = 9.4 Hz), 7.83 (t, 1H, H-6′, $J$ = 7.4 Hz), 4.96 (d, 1H, β-anomeric proton, $J$ = 7.8 Hz), 3.0–3.6 (m, 6H, glucosidic C—H); $^{13}$C NMR (100 MHz, Aseton-$d_6$, TMS, $\delta$ ppm): 155.44 (C-2), 138.59 (C-3), 173.84 (C-4), 128.42/128.31 (C-5, $^3J_{CF}$ = 11 Hz), 114.28/114.05 (C-6, $^2J_{CF}$ = 23 Hz), 167.07/164.60 (C-7, $^1J_{CF}$ = 252 Hz), 105.07/104.81 (C-8, $^2J_{CF}$ = 26 Hz), 156.83/156.69 (C-9, $^3J_{CF}$ = 14 Hz), 120.93 (C-10), 118.99/118.85 (C-1′, $^2J_{CF}$ = 14 Hz), 161.22/158.72 (C-2′, $^1J_{CF}$ = 250 Hz),115.90/115.69 (C-3′, $^2J_{CF}$ = 21 Hz), 133.02/132.93 (C-4′, $^3J_{CF}$ = 9 Hz), 124.09/125.05 (C-5′, $^4J_{CF}$ = 4 Hz),132.33/132.30 (C-6′, $^3J_{CF}$ = 3 Hz), 103.70 (β-anomeric carbon), 74.21 (Glu/C-2), 76.87 (Glu/C-3), 70.20 (Glu/C-4), 76.92 (Glu/C-5), 61.77 (Glu/C-6); HRMS (ESI-QTOF, positive) $m/z$ calcd for $C_{21}H_{18}F_2O_8$ [M + H]$^+$: 437.0970, found: 437.1005.

#### 4.7.11. 2-(3-fluorophenyl)-7-fluoro-3-O-β-D-glucopyranosyl-4H-chromen-4-one (5k)

Yellow solid; yield: 20 %; Mp: 185–186 °C; IR ($\nu_{max}$/cm$^{-1}$): 3324 (OH), 2954 (glucisidic C—H), 2925 (aliphatic C—H), 1612 (C═O), 1448 (C═C), 1188 (C—F), 1040 (C—O), 851 (β-configuration of anomeric carbon); $^1$H NMR (400 MHz, Aseton-$d_6$, TMS, $\delta$ ppm): 8.12 (dd, 1H, H-5, $J$ = 14.8/6.4 Hz), 7.22 (m, 1H, H-6), 7.47 (m, 1H, H-8), 7.95 (m, 2H, H-2′/6′), 7.22 (m, 1H, H-3′), 7.47 (m, 1H, H-5′), 5.29 (d, 1H, β-anomeric proton, $J$ = 7.8 Hz), 2.8–3.6 (m, 6H, glucosidic C—H); $^{13}$C NMR (100 MHz, Aseton-$d_6$, TMS, $\delta$ ppm): 137.65 (C-2), 133.73 (C-3), 173.96 (C-4), 128.27/128.16 (C-5, $^3J_{CF}$ = 11 Hz), 116.25/116.01 (C-6, $^2J_{CF}$ = 24 Hz), 167.09/164.57 (C-7, $^1J_{CF}$ = 251 Hz), 105.09/104.83 (C-8, $^2J_{CF}$ = 26 Hz), 156.47/156.33 (C-9, $^3J_{CF}$ = 14 Hz), 118.11 (C-10), 120.62 (C-1′),

114.13/113.90 (C-2′, $^{2}J_{CF}$ = 23 Hz), 163.38/160.94 (C-3′, $^{1}J_{CF}$ = 242 Hz),117.69/117.49 (C-4′, $^{2}J_{CF}$ = 21 Hz), 130.16/130.08 (C-5′, $^{3}J_{CF}$ = 8 Hz), 125.31/125.28 (C-6′, $^{4}J_{CF}$ = 3 Hz), 103.24 (β-anomeric carbon), 74.51 (Glu/C-2), 77.18 (Glu/C-3), 70.37 (Glu/C-4), 77.23 (Glu/C-5), 61.88 (Glu/C-6); HRMS (ESI-QTOF, positive) *m/z* calcd for $C_{21}H_{18}F_2O_8$ $[M + H]^+$: 437.0970, found: 437.1016.

#### *4.7.12. 2-(4-fluorophenyl)-7-fluoro-3-O-β-D-glucopyranosyl-4H-chromen-4-one (**5l**)*

Pale yellow powder; yield: 27 %; Mp: 204–205 °C; IR ($\nu_{max}$/cm$^{-1}$): 3378 (OH), 2951 (glucosidic C—H), 2925 (aliphatic C—H), 1614 (C═O), 1442 (C═C), 1167 (C—F), 1056 (C—O), 842 (β-configuration of anomeric carbon); $^{1}$H NMR (400 MHz, DMSO/$CDCl_3$, TMS, $\delta$ ppm): 8.17 (dd, 1H, H-5, $J$ = 15.3/6.4 Hz), 7.38 (m, 1H, H-6), 7.70 (d, 1H, H-8, $J$ = 9.6 Hz), 8.23 (dd, 2H, H-2′/6′, $J$ = 14.7/5.4 Hz), 7.38 (m, 2H, H-3′/5′), 5.54 (d, 1H, β-anomeric proton, $J$ = 7.7 Hz), 3.0–3.6 (m, 6H, glucosidic C—H), 4.2–5.5 (m, 4OH, glucosidic OH); $^{13}$C NMR (100 MHz, DMSO/$CDCl_3$, TMS, $\delta$ ppm): 155.63 (C-2), 136.70 (C-3), 173.39 (C-4), 128.43/128.32 (C-5, $^{3}J_{CF}$ = 11 Hz), 114.58/114.35 (C-6, $^{2}J_{CF}$ = 23 Hz), 166.73/164.91 (C-7, $^{1}J_{CF}$ = 182 Hz), 105.69/105.43 (C-8, $^{2}J_{CF}$ = 26 Hz), 156.20/156.12 (C-9, $^{3}J_{CF}$ = 8 Hz), 120.96 (C-10), 127.38 (C-1′), 132.16/132.07 (C-2′/6′, $^{3}J_{CF}$ = 9 Hz), 115.89/115.67 (C-3′/5′, $^{2}J_{CF}$ = 22 Hz), 164.23/162.55 (C-4′, $^{1}J_{CF}$ = 168 Hz), 101.19 (β-anomeric carbon), 74.55 (Glu/C-2), 76.86 (Glu/C-3), 70.23 (Glu/C-4), 77.96 (Glu/C-5), 61.36 (Glu/C-6); HRMS (ESI-QTOF, positive) *m/z* calcd for $C_{21}H_{18}F_2O_8$ $[M + H]^+$: 437.0970, found: 437.1008.

#### *4.7.13. 2-(2-chlorophenyl)-7-fluoro-3-O-β-D-glucopyranosyl-4H-chromen-4-one (**5m**)*

Yellow solid; yield: 25 %; Mp: 125–126 °C; IR ($\nu_{max}$/cm$^{-1}$): 3315 (OH), 2948 (glucosidic C—H), 2919 (aliphatic C—H), 1614 (C═O), 1446 (C═C), 1205 (C—F), 1060 (C—O), 855 (β-configuration of anomeric carbon); $^{1}$H NMR (400 MHz, Aseton-$d_6$, TMS, $\delta$ ppm): 8.16 (dd, 1H, H-5, $J$ = 14.8/6.4 Hz), 7.25 (d, 1H, H-6, $J$ = 8.0 Hz), 7.36 (m, 1H, H-8), 7.48 (m, 2H, H-3′/4′), 7.36 (m, 1H, H-5′), 7.79 (d, 1H, H-6′, $J$ = 7.8 Hz), 4.92 (d, 1H, β-anomeric proton, $J$ = 7.8 Hz), 3.0–3.6 (m, 6H, glucosidic C—H); $^{13}$C NMR (100 MHz, Aseton-$d_6$, TMS, $\delta$ ppm): 157.65 (C-2), 138.33 (C-3), 174.11 (C-4), 128.42/128.32 (C-5, $^{3}J_{CF}$ = 11 Hz), 114.34/114.11 (C-6, $^{2}J_{CF}$ = 23 Hz), 167.14/164.75 (C-7, $^{1}J_{CF}$ = 252 Hz), 105.05/104.90 (C-8, $^{2}J_{CF}$ = 25 Hz), 156.81/156.66 (C-9, $^{3}J_{CF}$ = 14 Hz), 120.93 (C-10), 129.78 (C-1′), 133.27 (C-2′),132.11 (C-3′), 132.86 (C-4′), 129.47 (C-5′),126.82 (C-6′), 103.72 (β-anomeric carbon), 74.24 (Glu/C-2), 76.88 (Glu/C-3), 70.17 (Glu/C-4), 76.94 (Glu/C-5), 61.59 (Glu/C-6); HRMS (ESI-QTOF, positive) *m/z* calcd for $C_{21}H_{18}ClFO_8$ $[M + H]^+$: 453.0674, found: 453.0708.

#### *4.7.14. 2-(3-chlorophenyl)-7-fluoro-3-O-β-D-glucopyranosyl-4H-chromen-4-one (**5n**)*

Light yellow powder; yield: 29 %; Mp: 175–176 °C; IR ($\nu_{max}$/cm$^{-1}$): 3346 (OH), 2951 (glucosidic C—H), 2917 (aliphatic C—H), 1613 (C═O), 1446 (C═C), 1203 (C—F), 1050 (C—O), 848 (β-configuration of anomeric carbon); $^{1}$H NMR (400 MHz, $CD_3OD$, TMS, $\delta$ ppm): 8.24 (m,1H, H-5), 7.29 (t, 1H, H-6, $J$ = 8.2 Hz,), 7.51 (m, 1H, H-8), 8.24 (m, 1H, H-2′), 7.51 (m, 2H, H-4′/5′), 8.09 (d, 1H, H-6′, $J$ = 6.8 Hz), 5.49 (d, 1H, β-anomeric proton, $J$ = 6.8 Hz), 3.0–4.0 (m, 6H, glucosidic C—H); $^{13}$C NMR (100 MHz, $CD_3OD$, TMS, $\delta$ ppm): 156.07 (C-2), 133.80 (C-3), 174.22 (C-4), 128.88/127.77 (C-5, $^{3}J_{CF}$ = 11 Hz), 113.92/113.69 (C-6, $^{2}J_{CF}$ = 23 Hz), 167.25/164.73 (C-7, $^{1}J_{CF}$ = 254 Hz), 104.67/104.41 (C-8, $^{2}J_{CF}$ = 25 Hz), 156.51/156.39 (C-9, $^{3}J_{CF}$ = 14 Hz), 120.58 (C-10), 132.29 (C-1′), 128.93 (C-2′), 137.09 (C-3′),129.47 (C-4′), 130.42 (C-5′), 127.27 (C-6′), 101.73 (β-anomeric carbon), 74.33 (Glu/C-2), 76.63 (Glu/C-3), 70.09 (Glu/C-4), 77.28 (Glu/C-5), 61.14 (Glu/C-6); HRMS (ESI-QTOF, positive) *m/z* calcd for $C_{21}H_{18}ClFO_8$ $[M + H]^+$: 453.0674, found: 453.0719.

#### *4.7.15. 2-(4-chlorophenyl)-7-fluoro-3-O-β-D-glucopyranosyl-4H-chromen-4-one (**5o**)*

Yellow solid; yield: 24 %; Mp: 197–198 °C; IR ($\nu_{max}$/cm$^{-1}$): 3339 (OH), 2955 (glucosidic C—H), 2925 (aliphatic C—H), 1611 (C═O), 1446 (C═C), 1204 (C—F), 1057 (C—O), 852 (β-configuration of anomeric carbon); $^{1}$H NMR (400 MHz, $CD_3OD$, TMS, $\delta$ ppm): 8.13 (m,1H, H-5), 7.19 (t, 1H, H-6, $J$ = 7.9 Hz), 7.37 (d, 1H, H-8, $J$ = 8.2 Hz,), 8.08 (d, 2H, H-2′/6′, $J$ = 8.8 Hz), 7.43 (d, 2H, H-3′/5′, $J$ = 8.8 Hz), 5.32 (d, 1H, β-anomeric proton, $J$ = 7.6 Hz), 3.0–3.6 (m, 6H, glucosidic C—H); $^{13}$C NMR (100 MHz, $CD_3OD$, TMS, $\delta$ ppm): 156.39 (C-2), 136.68 (C-3), 174.25 (C-4), 127.88/127.77 (C-5, $^{3}J_{CF}$ = 11 Hz), 113.88/113.65 (C-6, $^{2}J_{CF}$ = 23 Hz), 167.26/164.73 (C-7, $^{1}J_{CF}$ = 253 Hz), 104.59/104.34 (C-8, $^{2}J_{CF}$ = 25 Hz), 156.60/156.52 (C-9, $^{3}J_{CF}$ = 8 Hz), 120.57 (C-10), 129.17 (C-1′), 130.64 (C-2′/6′), 128.12 (C-3′/5′), 137.00 (C-4′), 101.92 (β-anomeric carbon), 74.27 (Glu/C-2), 76.61 (Glu/C-3), 69.91 (Glu/C-4), 77.21 (Glu/C-5), 61.11 (Glu/C-6); HRMS (ESI-QTOF, positive) *m/z* calcd for $C_{21}H_{18}ClFO_8$ $[M + H]^+$: 453.0674, found: 453.0684.

#### *4.7.16. 2-(2-bromophenyl)-7-fluoro-3-O-β-D-glucopyranosyl-4H-chromen-4-one (**5p**)*

Yellow oil; yield: 23 %; IR ($\nu_{max}$/cm$^{-1}$): 3351 (OH), 2950 (glucosidic C—H), 2925 (aliphatic C—H), 1617 (C═O), 1444 (C═C), 1202 (C—F), 1067 (C—O), 852 (β-configuration of anomeric carbon); $^{1}$H NMR (400 MHz, $CD_3OD$, TMS, $\delta$ ppm): 8.17 (dd, 1H, H-5, $J$ = 15.2/6.2 Hz), 7.20 (t, 1H, H-6, $J$ = 7.8 Hz), 7.35 (m, 1H, H-8), 7.62 (d, 1H, H-3′, $J$ = 7.8 Hz), 7.35 (m, 2H, H-4′/5′), 7.70 (d, 1H, H-6′, $J$ = 7.4 Hz), 5.05 (d, 1H, β-anomerik proton, $J$ = 7.8 Hz), 3.0–4.0 (m, 6H, glucosidic C—H); $^{13}$C NMR (100 MHz, $CD_3OD$, TMS, $\delta$ ppm): 158.73 (C-2), 137.79 (C-3), 174.36 (C-4), 128.04/127.93 (C-5, $^{3}J_{CF}$ = 11 Hz), 114.09/113.85 (C-6, $^{2}J_{CF}$ = 23 Hz), 167.33/164.80 (C-7, $^{1}J_{CF}$ = 253 Hz), 104.70/104.50 (C-8, $^{2}J_{CF}$ = 26 Hz), 156.78/156.65 (C-9, $^{3}J_{CF}$ = 13 Hz), 120.90 (C-10), 131.62 (C-1′), 122.36 (C-2′),132.61 (C-3′), 132.48 (C-4′), 131.80 (C-5′),126.94 (C-6′), 102.37 (β-anomeric carbon), 74.00 (Glu/C-2), 76.44 (Glu/C-3), 69.75 (Glu/C-4), 76.95 (Glu/C-5), 61.07 (Glu/C-6); HRMS (ESI-QTOF, positive) *m/z* calcd for $C_{21}H_{18}BrFO_8$ $[M + H]^+$: 497.0169, found: 497.0224.

#### *4.7.17. 2-(3-bromophenyl)-7-fluoro-3-O-β-D-glucopyranosyl-4H-chromen-4-one (**5q**)*

Bright yellow powder; yield: 25 %; Mp: 145–146 °C; IR ($\nu_{max}$/cm$^{-1}$): 3264 (OH), 2958 (glucosidic C—H), 2922 (aliphatic C—H), 1604 (C═O), 1455 (C═C), 1204 (C—F), 1165 (C—O), 890 (β-configuration of anomeric carbon); $^{1}$H NMR (400 MHz, $CD_3OD$, TMS, $\delta$ ppm): 8.01 (d, 1H, H-5, $J$ = 7.8 Hz), 7.18 (t, 1H, H-6, $J$ = 7.2 Hz), 7.34 (m, 1H, H-8), 8.24 (s, 1H, H-2′), 7.56 (d, 1H, H-4′, $J$ = 7.9 Hz), 7.34 (m, 1H, H-5′), 8.12 (dd, 1H, H-6′, $J$ = 15.2/6.0 Hz), 5.39 (d, 1H, β-anomeric proton, $J$ = 7.6 Hz), 3.0–3.8 (m, 6H, glucosidic C—H); $^{13}$C NMR (100 MHz, $CD_3OD$, TMS, $\delta$ ppm): 156.02 (C-2), 137.04 (C-3), 174.20 (C-4), 127.86/127.76 (C-5, $^{3}J_{CF}$ = 11 Hz), 113.91/113.68 (C-6, $^{2}J_{CF}$ = 24 Hz), 167.26/164.74 (C-7, $^{1}J_{CF}$ = 252 Hz), 104.66/104.53 (C-8, $^{2}J_{CF}$ = 26 Hz), 156.54/156.40 (C-9, $^{3}J_{CF}$ = 13 Hz), 120.62 (C-10), 132.53 (C-1′), 133.37 (C-2′), 121.64 (C-3′), 131.89 (C-4′), 129.68 (C-5′), 127.63 (C-6′), 101.64 (β-anomeric carbon), 74.33 (Glu/C-2), 76.51 (Glu/C-3), 70.12 (Glu/C-4), 77.30 (Glu/C-5), 61.36 (Glu/C-6); HRMS (ESI-QTOF, positive) *m/z* calcd for $C_{21}H_{18}BrFO_8$ $[M + H]^+$: 497.0169, found: 497.0186.

#### *4.7.18. 2-(4-bromophenyl)-7-fluoro-3-O-β-D-glucopyranosyl-4H-chromen-4-one (**5r**)*

Yellow powder; yield: 21 %; Mp: 203–204 °C; IR ($\nu_{max}$/cm$^{-1}$): 3359 (OH), 2954 (glucosidic C—H), 2933 (aliphatic C—H), 1608 (C═O), 1445 (C═C), 1204 (C—F), 1059 (C—O), 851 (β-configuration of anomeric carbon); $^{1}$H NMR (400 MHz, $CD_3OD$, TMS, $\delta$ ppm): 8.12 (dd, 1H, H-5, $J$ = 15.2/6.2 Hz), 7.19 (t, 1H, H-6, $J$ = 8.2 Hz), 7.36 (d, 1H, H-8, $J$ = 6.9 Hz), 8.0 (d, 2H, H-2′/6′, $J$ = 6.8 Hz), 7.58 (d, 2H, H-3′/5′, $J$ = 6.7 Hz), 5.32 (d, 1H, β-anomeric proton, $J$ = 7.6 Hz), 3.0–3.8 (m, 6H, glucosidic C—H); $^{13}$C NMR (100 MHz, $CD_3OD$, TMS, $\delta$ ppm): 156.37 (C-

2), 137.01 (C-3), 174.23 (C-4), 127.89/127.78 (C-5, $^{3}J_{CF}$ = 11 Hz), 113.89/113.66 (C-6, $^{2}J_{CF}$ = 23 Hz), 167.26/164.73 (C-7, $^{1}J_{CF}$ = 253 Hz), 104.60/104.34 (C-8, $^{2}J_{CF}$ = 26 Hz), 156.63/156.51 (C-9, $^{3}J_{CF}$ = 12 Hz), 120.56 (C-10), 129.57 (C-1′), 130.76 (C-2′/6′), 131.17 (C-3′/6′), 125.04 (C-4′), 101.90 (β-anomeric carbon), 74.32 (Glu/C-2), 76.60 (Glu/C-3), 69.90 (Glu/C-4), 77.21 (Glu/C-5), 61.11 (Glu/C-6); HRMS (ESI-QTOF, positive) *m/z* calcd for $C_{21}H_{18}BrFO_8$ $[M + H]^+$: 497.0169, found: 497.0242.

### 4.8. Molecular modeling

#### 4.8.1. Molecular docking

Molecular docking, also known as structure-based drug design, is a computer-aided drug development technique used to study how chemical molecules interact with target macromolecules (enzymes, nucleic acids, receptor proteins) for which three-dimensional structural information is available. It aims to predict the affinity of small molecule drug candidates to protein targets, their binding to these macromolecules and thus their biological activity. Studying the types of bond that are crucial for molecular interactions (such as hydrogen bonds, van der Waals, electrostatic bonds) enables the development of more effective and specific ligands [66,67].

In this study, molecular docking was used to investigate the interaction mechanism between flavonol-3-*O*-glucoside derivatives (**5a–r**) and SARS-CoV-2 3CLpro. The 3-dimensional (3D) crystal structure of SARS-CoV-2 3CLpro, containing the N3 inhibitor with the PDB code 6LU7 (resolution: 2.16 Å), was selected. Water and ion molecules were removed from this crystal structure, and missing hydrogen atoms and atomic charges were added using the program APBS-PDB2PQR [68]. A 40x40x40 lattice array with a lattice spacing of 0.375 Å was then defined, which included binding site of the target structure. A total of 100 independent runs per ligand were performed using the Lamarck genetic algorithm. The biomolecular target structure and ligand molecules were prepared according to the predetermined procedures, and molecular docking was performed using the AutoDock 4.2 program [69]. As a result of this process, the binding free energy (ΔG) and binding affinity were calculated for each possible conformation.

#### 4.8.2. Molecular dynamic simulation

A 100 ns molecular dynamics (MD) simulation was performed using Desmond software [70] to evaluate the binding stability of the most active compound 5a, and the reference compound in complex with the SARS-CoV-2 3CLpro protein. The Maestro 13.8 graphical interface integrated with the Desmond software configured the simulation parameters. The protein-ligand complex structures were placed in an orthorhombic simulation box and solvated using the TIP3P water model [71]. $Na^+$ and $Cl^-$ ions were added at a physiological concentration of 0.15 M to neutralize the system. The OPLS4 force field was applied to describe the molecular interactions of the protein-ligand complex.

The simulations were conducted under the NPT ensemble, maintaining a constant number of particles, a pressure of 1.01325 bar, and a temperature of 300 K. The Nosé–Hoover thermostat was utilized to control temperature, while the Martyna–Tobias–Klein method ensured stable pressure. Long-range electrostatic interactions were calculated using the Particle Mesh Ewald (PME) method. In contrast, short-range electrostatic and van der Waals interactions were limited to a cutoff distance of 9.0 Å [72], ensuring an accurate representation of intermolecular forces.

Comprehensive trajectory analyses were performed to investigate the dynamic behavior and stability of the protein-ligand complex. Key structural properties such as Root Mean Square Deviation (RMSD) and Root Mean Square Fluctuation (RMSF) were calculated, alongside binding interaction assessments, including hydrogen bonds and hydrophobic contacts. Additionally, dynamic properties such as molecular diffusion and conformational changes were examined.

The analysis of interactions between the protein and ligand further elucidated binding characteristics, focusing on critical non-covalent interactions, including hydrogen bonds, hydrophobic interactions, ionic interactions, and water bridges. These insights contribute to understanding the molecular mechanisms driving protein-ligand binding, thereby informing structure-based drug design and enabling the identification of potential optimization sites for enhancing ligand efficacy.

### 4.9. Antimicrobial activity

For the antimicrobial activity test, we used Mueller Hinton medium for the culture of *Escherichia coli*, *Yersinia pseudotuberculosis*, *Peusodomonas aeruginosa*, *Staphylococcus aureus*, *E. faecalis*, *Bacillus cereus* strains. The antituberculosis activity was tested against *Mycobacterium smegmatis* and BHI medium was used for cultivation. Cultures and PDA medium were used against yeasts, *Candida albicans* and *Saccharomyces cerevisiae*. To ensure the accuracy of our results, we thoroughly activated the pathogenic test bacteria in the appropriate media using the waxed jar method at 37 °C (yeasts at 28 °C) for 18 h. The final concentration of the cultures was adjusted to 0.5 McFarland. All active bacteria were homogeneously transferred to ELISA plates (96 wells) using a sterile swab stick and set aside. The inhibitory activities of the individual target compounds (**5a–r**) against selected pathogenic bacterial strains were tested. The compounds were transferred to the ELISA plates containing the selected pathogenic bacteria under aseptic conditions. Three antibiotics (ampicillin, streptomycin, fluconazole) were used as positive control. The antimicrobial activity was evaluated based on the growth observed in the wells after 24 h of incubation (Table 2) [73].

### 4.10. Inhibition study for COVID-19

#### 4.10.1. Investigation of the inhibitory effects of the compounds on the SARS-CoV-2 3CL protease

The determination of the inhibitory effect of the flavonol-3-*O*-glycoside, which was synthesized and their structures analyzed, on SARS-CoV-2 3CL protease was tested spectrophotometrically using a commercially developed kit (BPS Bioscience Cat No: 78042-1). In the study, the experimental buffer was prepared by adding DTT from a 0.5 M stock to the protease buffer with a final DTT concentration of 1 mM. Then the 3CL protease enzyme, which was included in the kit, was diluted with the buffer at a concentration of 0.5 ng/μL. Then 30 μL of the enzyme (in buffer) was added to each well (except blank). Only 10 μL of test buffer (with DTT) was added to the blank. 10 μL of the 3CL protease inhibitor (GC376 (500 μM)) supplied with the kit was added to the inhibitor control box. 10 μL of the test buffer (without DTT) was added to the positive control well. 10 μL of the substrate solution (containing 3CL protease substrate (10 mM) and 1.25 mL of assay buffer with DTT) was added to each well. 10 μL of each product was added to the wells of the synthesis products to be tested. Two replicates were planned for each group. The plate was then allowed to stand for 4 h at room temperature with gentle shaking. The fluorescence was then measured with a spectrophotometer (Spectramax M5) using 360 nm excitation and 460 nm emission values, analyzed and the $IC_{50}$ values calculated. The concentration range of the tested synthesis products was prepared in different stages and the $IC_{50}$ values were calculated for the lower concentration range [74–76].

#### 4.10.2. Studies to determine the nuclease activity

After investigating the inhibitory effect of the compounds whose synthesis was performed and whose structures were analyzed on the SARS-CoV-2 3CL protease, the nuclease activities of the compounds that showed good activity were investigated [75,76]. In the study, it was planned to use nucleic acids from different sources in the preliminary study, as it is very difficult to obtain COVID nucleic acid, it is costly and can only be obtained in limited quantities. Bacterial DNA (*Escherichia coli*) is an easy nucleic acid to obtain. Total chromosomal DNA was isolated and the antinuclease activity of the substances was tested. Since

nuclease activity against viral nucleic acid was planned in the study, a viral nucleic acid was also considered. For this purpose, AmF*V* virüs DNA obtained from Samsun Veterinary Control Institute Bee Diseases Research Laboratory (Vet. Dr. Rahşan AKPINAR) was used. The efficacy of substances acting on the nucleic acids of these two different microorganisms was tested against the nucleic acid of the COVID virus.

DNA activity was performed using undiluted stock concentrations of the chemicals. The starting materials were then diluted with sterile distilled water containing 1 % DMSO. Three different DNA nucleases were used for this activity. These were genomic DNA of the *E. coli* ATCC 25922 strain, of the filamentous virüs (AmFV) of the honey bee (*Apis mellifera*), and PCR product DNA of the N1 gene (N gene SARS-CoV-2_IBS_m_N 1 forward primer AAGGAAATTTTGGGGACCAG, reverse primer GAGTCAGCACTGCTCATGGA, 399 bp.), which was amplified from the cDNA of the COVID-19 OMICRON-BA1 strain [77].

Nuclease activity was induced with chemicals by incubation at 37 °C and 340 rpm shaking for 30, 60, 120, 180 and 240 min. After incubations 30, 60, 120, 180 and 240 min, 20 μl of sample (pH 5.0–6.5) was collected and run on a 1 % agarose gel at 60 V. The DNA was visualized with a UV transilluminator at a wavelength of 360 nm and photographed. Nuclease activity was assessed by comparing the DNA bands with the control band. Nuclease activity was scored on a scale of 0–4. The DNA that was not exposed to the nuclease activity and the control DNA were scored 4+, while the DNA fragmented by the nuclease activity was scored 0.

*4.10.2.1. E. coli genomic dsDNA study.* In the study, the main starting material was used directly for the experiment. The starting material was prepared using sterile distilled water with 1 % DMSO. The genomic DNA of the *E. coli* strain was extracted according to the method used by Sambrook et al. [69]. The obtained dsDNA products were examined by 1 % (*w/v*) agarose gel electrophoresis and visualized in a UV transilluminator.

The 10 compounds with the best enzyme activity were tested for nuclease activity. The 80 μl of 1 % solution of the experimental stock chemicals were taken and 20 μl nucleic acid was added to them. As a control, 20 μl of *E. coli* DNA was added to 80 μl of sterile distilled water and used as negative control (NK). NK: This was a control DNA study and 80 μl of sterile distilled water was used. 20 μl of DNA were added directly, and DNA without chemical treatment was used as a negative control.

After the samples were treated with DNA, they were stored for 30, 60, 120, 180 and 240 min. It was kept at 37 °C and 340 rpm and shaken at intervals. At each expiration date, 20 μl were collected and run on a 1 % agarose gel at 60 V. Observed and photographed at 360 nm wavelength with a UV transilluminator. The pH values of the substances were measured by dripping them with pH strips before the experiment.

*4.10.2.2. Examination of bee virus DNA (filamentous virus, bp 551).* *Apis mellifera* filamentous virus (AmFV) is a major virus of honey bees that contains a double-stranded DNA genome, but its relationship to other parasites and its distrubition are poorly understood. The viral double-stranded DNA genome is encapsidated in a long nucleocapsid 3000 × 40 nm in lenght, and enclosed in a membrane. The first molecular diagnosis of the AmFV virus revealed that it is widespread in honey bee colonies and is probably transmitted both horizontally through food exchange and vertically from the queen to the workers. Acute infections of honey bees with AmFV lead to degradation of bee tissues, such as the fat body, resulting in characteristic symptoms in which the hemolymph of workers appears milky white [78]. This nucleic acid; double-stranded DNA was considered as a model to observe its activity against viral nucleic acids. Viral DNA amplified by PCR with specific primers was used for the study.

RNA extraction from tissue: 15 samples of adult bee from the same hive were transferred to 7 mL cryotubes and 3 mL of PBS (SIGMA, 806544-500 mL, USA) was added. Then the samples were homogenized in an automatic homogenizer (Bead Ruptor Elite, Bead Mill Homogenizer, SKU 19-042E, OMNI International, USA). After the homogenization process, the samples were centrifuged at 4000 rpm at +4 °C for 15 min and then the RNA was extracted from the supernatant. Remaining samples were stored at −20 °C. RNA extraction was performed using a commercial kit (High Pure Viral Nucleic Acid Kit, REF: 11858874001, Roche, Germany) according to the manufacturer's instructions. The extracted RNAs were stored at −20 °C until testing.

Diagnostic PCR primers were selected for the region encoding the Bro gene (AmFV_112: forward CAGAGAATTCGGTTTTTGTGAGTG and reverse CATGGTGGCCAAGTCTTGCT) of the AmFV genome. PCR reactions were using with standard reagents containing 0.4 μM of each primer and a cycling profile of 30 min at 50 °C, followed by 15 min at 95 °C, 1 min at 94 °C, 1 min at 55 °C, and 72 min at 50 °C. It was performed with 40 cycles of 1 min at °C. The identity of the PCR amplicons was confirmed by Sanger sequencing [79].

In the study, the 10 compounds with the best enzyme activity were tested for nuclease activity. The 20 μl of each stock sample were placed in 3 separate tubes and 5 μl of DNA were added. The first series was kept on a vibrating hot plate at 37 °C for half an hour, then run on a 1 % agarose gel and images were taken. The second and third tubes were taken at 120 and 240 min and were run on a 1 % agarose gel and visualized with a UV transilluminator.

*4.10.2.3. Examination of the DNA of the COVID-19 virus.* The COVID virus has a single-stranded RNA genome with negative polarity. The RNA contains the bases adenine, guanine, uracil and cytosine, but also ribose-pentose as a sugar molecule. RNA is shorter and has a different structure to the DNA molecule. The isolation of RNA is very difficult. It is not as stable a molecule as DNA. As RNA is an unstable molecule, it breaks easily during isolation and decays very quickly. RNA can be isolated using four different methods. These methods are the “guanidine thiocyanate method”, the “proteinase K method”, the “cesium chloride gradient purification” and the “RNA isolation method with Trizol (combined method)”. RNA isolation should always be carried out in a cold environment (on ice). If the tubes are left outside for even 30 s during isolation, the RNAs will degrade. Isolated RNAs are stored at −80 °C. The RNA molecule can be run on agarose gel just like the DNA molecule. However, the buffers used and the environmental conditions are different. If the RNA is degraded when the whole RNA is isolated, a smear pattern is formed in the agarose gel. For all these reasons, it is difficult to use RNA as material for the nuclease activity experiment and the results are not objective. For this reason, the isolated RNAs were quickly converted into cDNA using the enzyme reverse transcriptase and then stable double-stranded DNA was obtained using complementary DNA.

Since it not possible to expose the COVID RNA to chemicals at 37 °C in our study, double-stranded DNA was used, which was amplified with cDNA was. However, since this procedure is also quite costly and the DNA obtained is limited, the DNA fragment amplified by PCR was used as test material. Using CO*V*ID-19 DNA specific primers (SARS-CoV-2-IBS-m-N1 Forward; AAGGAAATTTTGGGGACCAG and Reverse; GAGTCAGCACTGCTCATGGA) belonging to the COVID-19 Omikron B1 strain, fragments of 399 bp (Fig. 4) were obtained by conventional PCR technique [80].

In the study, the 4 compounds with the best DNase activity on *E. coli* and AmF*V* DNA were tested for COVID-19 nuclease activity. The 20 μl of each of the stock solutions of 4 different chemicals were added to 3 separate tubes and 5 μl of the DNA of the Omikron BA1 strain were added. The first series was kept on a vibrating hot plate at 37 °C for half an hour and then fixed in a 2 % agarose gel at 80 W for 20–30 min and photographed. The second and third tubes were taken at 120 and 240 min and were run on a 2 % agarose gel and visualized with a UV transilluminator.

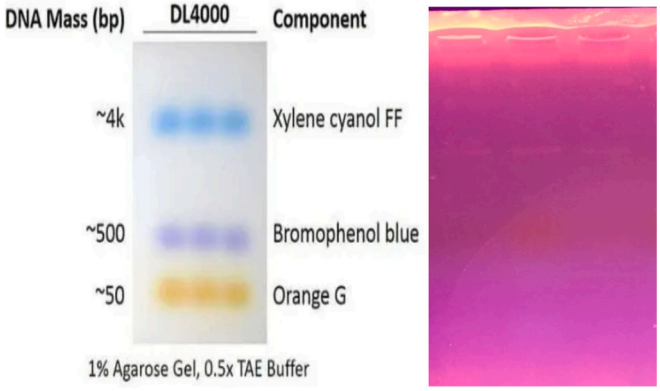


**Fig. 4.** Control dye (Orange G; 50 bp) and control COVID DNA (Omikron-BA1 strain 399 bp).

## CRediT authorship contribution statement

**Gonca Çelik:** Writing – original draft, Project administration, Methodology, Investigation, Formal analysis, Data curation. **Şengül Alpay Karaoğlu:** Supervision, Investigation, Funding acquisition, Data curation. **Şeyma Suyabatmaz:** Methodology, Conceptualization. **Arif Bozdeveci:** Methodology. **Gizem Tatar Yılmaz:** Methodology, Formal analysis. **Nurettin Yaylı:** Supervision, Data curation. **Rahşan Akpınar:** Methodology, Investigation. **Ayşegül Çopur Çiçek:** Methodology.

## Declaration of competing interest

The authors declare that they have no known competing financial interests or personal relationships that could have appeared to influence the work reported in this paper.

## Acknowledgements

The authors wish to express thanks to the Scientific and Technological Research Council of Turkey (TUBITAK, No. 121C188) for providing financial support. We are very much thankful to the Recep Tayyip Erdoğan University and Karadeniz Technical University for providing the research facilities. The numerical calculations were performed at The Scientific and Technological Research Council of Turkey (TUBITAK) ULAKBIM High Performance and Grid Computing Center (TRUBA resources). This computational study was supported by Karadeniz Technical University Scientific Research Projects (BAP) – Research Infrastructure Project (BAP04) by the (Project Number: TAY-2022-10040).

## Appendix A. Supplementary data

Supplementary data to this article can be found online at https://doi.org/10.1016/j.ijbiomac.2025.139621.

## References

[1] A. Jhanwar, D. Sharma, U. Das, Unraveling the structural and functional dimensions of SARS-CoV2 proteins in the context of COVID-19 pathogenesis and therapeutics, Int. J. Biol. Macromol. 278 (2024) 134850, https://doi.org/10.1016/j.ijbiomac.2024.134850.
[2] C.C. Lai, T.P. Shih, W.C. Ko, H.J. Tang, P.R. Hsueh, Severe acute respiratory syndrome coronavirus 2 (SARS-CoV-2) and coronavirus disease-2019 (COVID-19): the epidemic and the challenges, Int. J. Antimicrob. Agents 55 (3) (2020) 105924, https://doi.org/10.1016/j.ijantimicag.2020.105924.
[3] A.E. Gorbalenya, S.C. Baker, R.S. Baric, R.J. de Groot, C. Drosten, A.A. Gulyaeva, B. L. Haagmants, C. Lauber, A.M. Leontovich, B.W. Neuman, D. Penzar, S. Perlman, L. L.M. Poon, D.V. Samborskiy, I.A. Sidorov, I. Sola, J. Ziebuhr, The species severe acute respiratory syndrome-related coronavirus: classifying 2019-nCoV and naming it SARS-CoV-2, Nat. Microbiol. 5 (2020) 536–544, https://doi.org/10.1038/s41564-020-0695-z.
[4] WHO. https://www.who.int/emergencies/diseases/novel-coronavirus-2019/technicalguidance/naming-the-coronavirus-disease-(covid-2019)-and-the-virus-that-causes-it, 2020 (accessed 11 February 2020).
[5] L. Paulsson-Habegger, A.K. Snabaitis, S.P. Wren, Enzyme inhibition as a potential therapeutic strategy to treat COVID-19 infection, Bioorg. Med. Chem. 48 (2021) 116389, https://doi.org/10.1016/j.bmc.2021.116389.
[6] C. Huang, C. Yang, X. Xu, W. Xu, S. Liu, Structural and functional properties of SARS-CoV-2 spike protein: potential antivirus drug development for COVID-19, Acta Pharmacol. Sin. 41 (2020) 1141–1149, https://doi.org/10.1038/s41401-020-0485-4.
[7] WHO COVID-19 Dashboard. https://covid19.who.int/, 2024.
[8] Y. Vakulenko, A. Deviatkin, J.F. Drexler, A. Lukashev, Modular evolution of coronavirus genomes, Viruses 13 (2021) 1270, https://doi.org/10.3390/v13071270.
[9] W.K. Jo, E.F. de Oliveira-Filho, A. Rasche, A.D. Greenwood, K. Osterrieder, J. F. Drexler, Potential zoonotic sources of SARS-CoV-2 infections, Transbound. Emerg. Dis. 68 (4) (2020) 1824–1834, https://doi.org/10.1111/tbed.13872.
[10] D. Rout, A.K. Sahoo, Clinical implications of a mechanistic link connecting SARS-Cov-2, diabetes mellitus, zinc in COVID-19 pathophysiology, and the prophylactics in the treatment of SARS-CoV-2, Eur. J. Med. Chem. 9 (2023) 100117, https://doi.org/10.1016/j.ejmcr.2023.100117.
[11] F. Jiang, L. Deng, L. Zhang, Y. Cai, C.W. Cheung, Z. Xia, Review of the clinical characteristics of coronavirus disease 2019 (COVID-19), J. Gen. Intern. Med. 35 (2020) 1545–1549, https://doi.org/10.1007/s11606-020-05762-w.
[12] G.M. Vilke, J.J. Brennan, A.O. Cronin, E.M. Castillo, Clinical features of patients with COVID-19: is temperature screening useful? J. Emerg. Med. 59 (6) (2020) 952–956, https://doi.org/10.1016/j.jemermed.2020.09.048.
[13] B.D. Nuertey, K. Ekremet, A.R. Haidallah, K. Mumuni, J. Addai, R.I.E. Attibu, M. C. Damah, E. Duorinaa, A.S. Seidu, V.C. Adongo, R.K. Adatsi, H.C. Suri, A. A. Komei, B.B. Abubakari, E. Weyori, E. Allegye-Cudjoe, A. Sylverken, M. Owusu, R.O. Phillips, Performance of COVID-19 associated symptoms and temperature checking as a screening tool for SARS-CoV-2 infection, PloS One 16 (9) (2021) e0257450, https://doi.org/10.1371/journal.pone.0257450.
[14] L. Tian, T. Qiang, X. Yang, Y. Gao, X. Zhai, K. Kang, C. Du, Q. Lu, H. Gao, D. Zhang, X. Xie, C. Liang, Development of de-novo coronavirus 3-chymotrypsin-like protease (3CLpro) inhibitors since COVID-19 outbreak: a strategy to tackle challenges of persistent virus infection, Eur. J. Med. Chem. 264 (2024) 115979, https://doi.org/10.1016/j.ejmech.2023.115979.
[15] H. Yang, Z. Rao, Structural biology of SARS-CoV-2 and implications for therapeutic development, Nat. Rev. Microbiol. 19 (2021) 685–700, https://doi.org/10.1038/s41579-021-00630-8.
[16] L. Mousavizadeh, S. Ghasemi, Genotype and phenotype of COVID-19: their roles in pathogenesis, J. Microbiol. Immunol. Infect. 54 (2) (2021) 159–163, https://doi.org/10.1016/j.jmii.2020.03.022.
[17] R. Kumar, S. Mishra, S.K. Maurya Shreya, Recent advances in the discovery of potent RNA-dependent RNA-polymerase (RdRp) inhibitors targeting viruses, RSC, Med. Chem. 12 (3) (2020) 306–320, https://doi.org/10.1039/D0MD00318B.
[18] Sk. Abdul Amin, S. Banerjee, K. Ghosh, S. Gayen, T. Jha, Protease targeted COVID-19 drug discovery and its challenges: Insight into viral main protease (Mpro) and papain-like protease (PLpro) inhibitors, Bioorg. Med. Chem. 29 (2021) 115860, https://doi.org/10.1016/j.bmc.2020.115860.
[19] J.L. Vique-Sanchez, Potential inhibitors interacting in Neuropilin-1 to develop an adjuvant drug against COVID-19, by molecular docking, Bioorg. Med. Chem. 33 (2021) 116040, https://doi.org/10.1016/j.bmc.2021.116040.
[20] H. Yang, W. Xie, X. Xue, K. Yang, J. Ma, W. Liang, Q. Zhao, Z. Zhou, D. Pei, J. Ziebuhr, R. Hilgenfeld, K.Y. Yuen, L. Wong, G. Gao, S. Chen, Z. Chen, D. Ma, M. Bartlam, Z. Rao, Design of wide-spectrum inhibitors targeting coronavirus main proteases, PLoS Biol. 3 (10) (2005) e324, https://doi.org/10.1371/journal.pbio.0030324.
[21] J.D. Goldman, D.C.B. Lye, D.S. Hui, K.M. Marks, R. Bruno, R. Montejano, C. D. Spinner, M. Galli, M.Y. Ahn, R.G. Nahass, Y.S. Chen, D. SenGupta, R.H. Hyland, A.O. Osinusi, H. Cao, C. Blair, X. Wei, A. Gaggar, D.M. Brainard, W.J. Towner, J. Munoz, K.M. Mullane, F.M. Marty, K.T. Tashima, G. Diaz, A. Subramanian, Remdesivir for 5 or 10 days in patients with severe COVID-19, N. Engl. J. Med. 383 (19) (2020) 1827–1837, https://doi.org/10.1056/NEJMoa2015301.
[22] M.S. Khuroo, Chloroquine and hydroxychloroquine in coronavirus disease 2019 (COVID-19), facts, fiction, and hype: a critical appraisal, Int. J. Antimicrob. Agents 56 (3) (2020) 106101, https://doi.org/10.1016/j.ijantimicag.2020.106101. Get rights and content.
[23] Q. Cai, M. Yang, D. Liu, J. Chen, D. Shu, J. Xia, X. Liao, Y. Gu, Q. Cai, Y. Yang, C. Shen, X. Li, L. Peng, D. Huang, J. Zhang, S. Zhang, F. Wang, J. Liu, L. Chen, S. Chen, Z. Wang, Z. Zhang, R. Cao, W. Zhong, Y. Liu, L. Liu, Experimental treatment with favipiravir for COVID-19: an open-label control study, Engineering 6 (10) (2020) 1192–1198, https://doi.org/10.1016/j.eng.2020.03.007.
[24] S. Ekins, T.R. Lane, P.B. Madrid, Tilorone: a broad-spectrum antiviral invented in the USA and commercialized in Russia and beyond, Pharm. Res. 37 (4) (2020) 71, https://doi.org/10.1007/s11095-020-02799-8.
[25] D. Huang, H. Yu, T. Wang, H. Yang, R. Yao, Z. Liang, Efficacy and safety of umifenovir for coronavirus disease 2019 (COVID-19): a systematic review and meta-analysis, J. Med. Virol. 93 (1) (2021) 481–490, https://doi.org/10.1002/jmv.26256.
[26] B. Dinda, M. Dinda, S. Dinda, M. Chakraborty, Some natural compounds and their analogues having potent anti-SARS-CoV-2 and anti-proteases activities as lead molecules in drug discovery for COVID-19, Eur. J. Med. Chem. 6 (2022) 100079, https://doi.org/10.1016/j.ejmcr.2022.100079.

[27] M. Li, Y. Du, L. Zhang, H. Wu, D. Zhao, Q. Wang, T. Wang, Synthesis and photochemistry of flavonol camphorsulfonates photoinitiator with different substituents, Prog. Org. Coat. 183 (2023) 107810, https://doi.org/10.1016/j.porgcoat.2023.107810.
[28] J.M. Garcia-Chacon, J.C. Marin-Loaiza, C. Osorio, Camu Camu (Myrciaria dubia (Kunth) McVaugh): an Amazonian fruit with biofunctional properties−a review, ACS Omega 8 (2023) 5169–5183, https://doi.org/10.1021/acsomega.2c07245.
[29] S. Gholomi, A.K. Bordbar, Exploring binding properties of naringenin with bovine β-lactoglobulin: a fluorescence, molecular docking and molecular dynamics simulation study, Biophys. Chem. 187-188 (2014) 33–42, https://doi.org/10.1016/j.bpc.2014.01.003.
[30] J. Ashraf, E.U. Mughala, A. Sadiqb, M. Bibia, N. Naeema, A. Alic, A. Massadaqc, N. Fatimad, A. Javida, M.N. Zafare, B.A. Khanf, M.F. Nazara, A. Mumtazg, M. N. Tahirh, M. Mirzaeii, Exploring 3-hydroxyflavone scaffolds as mushroom tyrosinase inhibitors: synthesis, X-ray crystallography, antimicrobial, fluorescence behaviour, structure-activity relationship and molecular modeling studies, J. Biomol. Struct. Dyn. 39 (18) (2021) 7107–7122, https://doi.org/10.1080/07391102.2020.1805364.
[31] Y. Lyu, S. Liu, S. Gao, J. Zhou, Identification and characterization of three flavonoid 3-Oglycosyltransferases from *Epimedium koreanum* Nakai, Biochem. Eng. J. 163 (2020) 107759, https://doi.org/10.1016/j.bej.2020.107759.
[32] M.P. Garcia-Mendoza, F.A. Espinosa-Pardo, R. Savoire, C. Harscoat-Schiavo, M. Cansell, P. Subra-Paternault, Improvement of the oxidative stability of camelina oil by enrichment with phospholipid-quercetin formulations, Food Chem. 341 (2021) 128234, https://doi.org/10.1016/j.foodchem.2020.128234.
[33] D. Narog, Electrochemical study of quercetin in the presence of galactopyranose: potential application to the electrosynthesis of glycoconjugates of quinone/quinone methide of quercetin, J. Electroanal. Chem. 878 (2020) 114675, https://doi.org/10.1016/j.jelechem.2020.114675.
[34] M.H.S. Al-Shabibi, S.S.J. Al-Touby, M.A. Hossain, Isolation, characterization and prediction of biologically active glycoside compounds quercetin-3-rutinoside from the fruits of Ficus sycomorus, Carbohydr. Res. 511 (2022) 108483, https://doi.org/10.1016/j.carres.2021.108483.
[35] E.O. Norman, H. Tuohey, D. Pizzi, M. Saidah, R. Bell, R. Brkljača, J.M. White, R. B. Gasser, A.C. Taki, S. Urban, Phytochemical profiling and biological activity of the Australian carnivorous plant, Drosera magna, J. Nat. Prod. 84 (4) (2021) 964–971, https://doi.org/10.1021/acs.jnatprod.0c00869.
[36] L. Chen, J. Li, C. Luo, H. Liu, W. Xu, G. Chen, O.W. Liew, W. Zhu, C.M. Puah, X. Shen, H. Jiang, Binding interaction of quercetin-3-β-galactiside and its synthetic derivatives with SARS-CoV $3CL^{pro}$: structure-activity relationship studies reveal salient pharmacophore features, Bioorg. Med. Chem. 14 (2006) 8295–8306, https://doi.org/10.1016/j.bmc.2006.09.014.
[37] P. Das, R. Majumder, M. Mandal, P. Basak, In-silico approach for identification of effective and stable inhibitors for COVID-19 main protease ($M^{pro}$) from flavonoid based phytochemical constituents of *Calendula officinalis*, J. Biomol. Struct. Dyn. 39 (16) (2021) 6265–6280, https://doi.org/10.1080/07391102.2020.1796799.
[38] G. Tosun, T. Arslan, Z. İskefiyeli, M. Küçük, Ş. Alpay Karaoğlu, N. Yaylı, Synthesis and biological evaluation of a new series of 4-alkoxy-2-arylquinoline derivatives as potential antituberculosis agents, Turk. J. Chem. 39 (2015) 850–866, https://doi.org/10.3906/kim-1501-112.
[39] X. Shen, Q. Zhou, W. Xiong, W. Pu, W. Zhang, G. Zhang, C. Wang, Synthesis of 5-substituted flavonols via the Algar-Flynn-Oyamada (AFO) reaction: the mechanistic implication, Tetrahedron 73 (2017) 4822–4829, https://doi.org/10.1016/j.tet.2017.06.064.
[40] J. Ashraf, E.U. Mughal, A. Sadiq, N. Naeem, S.A. Muhammad, T. Qousain, M. N. Zafar, B.A. Khan, M. Anees, Design and synthesis of new flavonols as dual α-amylase and α-glucoside inhibitors: structure-activity relationship, drug-likeness, *in-vitro* and *in-silico* studies, J. Mol. Struct. 1218 (2020) 128458, https://doi.org/10.1016/j.molstruc.2020.128458.
[41] V.N. Ingle, S.T. Kharche, U.G. Upadhyay, Glucosylation of 4′-hydroxychalcones using glucosyl donor, Indian J. Chem. Sect. B 44 (2005) 801. http://nopr.niscpr.res.in/handle/123456789/8985.
[42] G. Çelik, G. Tatar Yılmaz, H. Sahin, B. Barut, N. Yaylı, Design, synthesis, and enzyme inhibition evaluation of some novel mono- and di-*O*-β-D-glycopyranosyl chalcone analogues with molecular docking studies, Turk. J. Chem. 47 (1) (2023) 171–184, https://doi.org/10.55730/1300-0527.3527.
[43] M. Liu, P. Wilairat, S.L. Croft, A.L.C. Tan, M.L. Go, Structure-activity relationships of antileishmanial and antimalarial chalcones, Bioorg. Med. Chem. 11 (13) (2003) 2729–2738, https://doi.org/10.1016/S0968-0896(03)00233-5.
[44] A. Kurzwernhart, W. Kandioller, S. Baechler, C. Bartel, S. Martic, M. Buczkowska, G. Muehlgassner, M.A. Jakupec, H.B. Kraatz, P.J. Bednarski, V.B. Arion, D. Marko, B.K. Keppler, C.G. Hartinger, Structure-activity relationships of targeted RuII(η6-p-cymene) anticancer complexes with flavonol-derived ligands, J. Med. Chem. 55 (23) (2012) 10512–10522, https://doi.org/10.1021/jm301376a.
[45] M. Reszka, I.E. Serdiuk, K. Kozakiewicz, A. Nowacki, H. Myszka, P. Bojarski, B. Liberek, Influence of a 4′-substituent on the efficiency of flavonol-based fluorescent indicators of β-glycosidase activity, Org. Biomol. Chem. 18 (38) (2020) 7635–7648, https://doi.org/10.1039/D0OB01505A.
[46] N. Öztürk, G. Çelik, C. Alaşalvar, E. Temel, H. Gökce, Synthesis, structural, spectroscopic (NMR, FT-IR and UV–vis), NLO, *in silico* (ADMET and molecular docking) and DFT investigations of a flavonol derivative 2-(4-chlorophenyl)-7-fluoro-3-hydroxy-4H-chromen-4-one, J. Mol. Struct. 1322 (2025) 140490, https://doi.org/10.1016/j.molstruc.2024.140490.
[47] E.U. Mughal, A. Javid, A. Sadiq, S. Murtaza, M.N. Zafar, B.A. Khan, S.H. Sumrra, M. N. Tahir, K.M. Khan Kanwalf, Synthesis, structure-activity relationship and molecular docking studies of 3-O-flavonol glycosides as cholinesterase inhibitors, Bioorg. Med. Chem. 26 (2018) 3696–3706, https://doi.org/10.1016/j.bmc.2018.05.050.
[48] M. Ninomiya, M. Efdi, T. Inuzuka, M. Koketsu, Chalcone glycosides from aerial parts of Brassica rapa L. 'hidabeni', turnip, Phytochem. Lett. 3 (2010) 96–99, https://doi.org/10.1016/j.phytol.2010.02.004.
[49] E.U. Mughala, A. Sadiqb, M. Ayubb, N. Naeema, A. Javida, S.H. Sumrraa, M. N. Zafarc, B.A. Khand, F.P. Malikeand, I. Ahmed, Exploring 3-Benzyloxyflavones as new lead cholinesterase inhibitors: synthesis, structure–activity relationship and molecular modeling simulations, Biomol. Struct. Dyn. 39 (16) (2021) 6154–6167, https://doi.org/10.1080/07391102.2020.1803136.
[50] N. Yaylı, G. Kılıç, G. Çelik, N. Kahriman, Ş. Kanbolat, A. Bozdeveci, Ş. Alpay Karaoğlu, R. Aliyazıcıoğlu, H.E. Sellitepe, İ.S. Doğan, A. Aydın, Synthesis of Hydroxy benzoin/Benzil analogs and investigation of their antioxidant, antimicrobial, enzyme inhibition, and cytotoxic activities, Turk. J. Chem. 45 (3) (2021) 788–804, https://doi.org/10.3906/kim-2012-25.
[51] Z. Zhu, X. Feng, H. Wang, J. Fan, C. Zhang, G. Song, L. Tang, Design, synthesis and biological activity of coumarin-chalcone hybrid derivatives as phosphodiesterase type II (PDE2) inhibitors, Tetrahedron 149 (2023) 133733, https://doi.org/10.1016/j.tet.2023.133733.
[52] X. Shen, Q. Zhou, W. Xiong, W. Pu, W. Zhang, G. Zhang, C. Wang, Synthesis of 5-substituted flavonols via the Algar-Flynn-Oyamada (AFO) reaction: the mechanistic implication, Tetrahedron 73 (2017) 4822–4829, https://doi.org/10.1016/j.tet.2017.06.064.
[53] G. Çelik, New chalcone-3-O-glycoside derivatives: synthesis and characterization, J. Chem. Res. 44 (9–10) (2020) 598–601, https://doi.org/10.1177/1747519820915165.
[54] Z. Jin, X. Du, Y. Xu, Y. Deng, M. Liu, Y. Zhao, B. Zhang, X. Li, L. Zhang, C. Peng, Y. Duan, J. Yu, L. Wang, K. Yang, F. Liu, R. Jiang, X. Yang, T. You, X. Liu, X. Yang, F. Bai, H. Liu, L.W. Guddat, W. Xu, G. Xiao, C. Qin, Z. Shi, H. Jiang, Z. Rao, H. Yang, Structure of M pro from SARS-CoV-2 and discovery of its inhibitors, Nature 582 (7811) (2020) 289–293, https://doi.org/10.1038/s41586-020-2223-y.
[55] S. Ullrich, C. Nitsche, The SARS-CoV-2 main protease as drug target, Bioorg. Med. Chem. Lett. 30 (17) (2020) 127377, https://doi.org/10.1016/j.bmcl.2020.127377.
[56] S.A. Hollingsworth, R.O. Dror, Molecular dynamics simulation for all, Neuron 99 (2018) 1129–1143, https://doi.org/10.1016/j.neuron.2018.08.011.
[57] X. Mu, J. Wang, M. Sun, Two-dimensional black phosphorus: physical properties and applications, Mater. Today Phys. 8 (2019) 92–111, https://doi.org/10.1016/j.mtphys.2019.02.003.
[58] G. Çelik, G. Tatar Yılmaz, B. Barut, C.Ö. Yalçın, N. Yaylı, Design, synthesis, biological activity and molecular docking studies of new imine-chalcone derivatives, Pharm. Chem. J. 57 (4) (2023) 550–558, https://doi.org/10.1007/s11094-023-02919-9.
[59] M.L. Ma, M. Li, J.J. Gou, T.Y. Ruan, H.S. Jin, L.H. Zhang, L.C. Wu, X.Y. Li, Y.H. Hu, K. Wen, Z. Zhao, Design, synthesis and biological activity of flavonoid derivatives as selective agonists for neuromedin U 2 receptor, Bioorg. Med. Chem. 22 (21) (2014) 6117–6123, https://doi.org/10.1016/j.bmc.2014.08.038.
[60] G. Çelik, T. Arslan, M. Şentürk, D. Ekinci, Synthesis and characterization of some new pyrazolines and their inhibitory potencies against carbonic anhydrases, Arch. Pharm. 353 (2020) e1900292, https://doi.org/10.1002/ardp.201900292.
[61] L.S. Dhivya, M.K. Kathiravan, T. Gopalakrishnan, Design, synthesis and anti-Tb evaluation of chalcone derivatives as novel inhibitors of InhA, J. Biomol. Struct. Dyn. 41 (24) (2023) 15165–15176, https://doi.org/10.1080/07391102.2023.2227711.
[62] A.R. Jesus, A.P. Marques, A.P. Rauter, An easy approach to dihydrochalcones *via* chalcone *in situ* hydrogenation, Pure Appl. Chem. 88 (4) (2016) 349–361, https://doi.org/10.1515/pac-2016-0303.
[63] Y.X. Chen, C.H. Chang, C.W. Li, J.J. Chen, T.L. Shih, Design, synthesis, and evaluation of 1,2,3-triazole-basedbenzenesulfonamide and flavonol hybrid molecules asanticancer agents, J. Chin. Chem. Soc. 70 (2023) 1924–1936, https://doi.org/10.1002/jccs.202300279.
[64] T.A. Dias, C.L. Duarte, C.F. Lima, M.F. Proença, C. Pereira-Wilson, Superior anticancer activity of halogenated chalcones and flavonols over the natural flavonol quercetin, Eur. J. Med. Chem. 65 (2013) 500–510, https://doi.org/10.1016/j.ejmech.2013.04.064.
[65] J. Ashraf, E.U. Mughal, A. Sadiq, N. Naeem, S.A. Muhammad, T. Qousain, M. N. Zafar, B.A. Khan, M. Anees, Design and synthesis of new flavonols as dual α-amylase and α-glucoside inhibitors: structure-activity relationship, drug-likeness, *in-vitro* and *in-silico* studies, J. Mol. Struct. 1218 (2020) 128458, https://doi.org/10.1016/j.molstruc.2020.128458.
[66] D.B. Kitchen, H. Decornez, J.R. Furr, J. Bajorath, Docking and scoring in virtual screening for drug discovery: methods and applications, Nat. Rev. Drug Discov. 3 (11) (2004) 935–949, https://doi.org/10.1038/nrd1549.
[67] T. Lengauer, M. Rarey, Computational methods for biomolecular docking, Curr. Opin. Struct. Biol. 6 (3) (1996) 402–406, https://doi.org/10.1016/S0959-440X(96)80061-3.
[68] E. Jurrus, D. Engel, K. Star, K. Monson, J. Brandi, L.E. Felberg, D.H. Brookes, L. Wilson, J. Chen, K. Liles, M. Chun, P. Li, D.W. Gohara, T. Dolinsky, R. Konecny, D.R. Koes, J.E. Nielsen, T. Head-Gordon, W. Geng, R. Krasny, G.W. Wei, M.J. Holst, J.A. McCammon, N.A. Baker, Improvements to the APBS biomolecular solvation software suite, Protein Sci. 27 (2018) 112–128, https://doi.org/10.1002/pro.3280.
[69] J. Sambrook, D.W. Russell, Molecular Cloning: A Laboratory Manual 3rd edition, Vol. 1, Cold Spring Harbor Laboratory Press, New York, 2001.
[70] L.L.C. Schrodinger, Schrödinger Release 2023–4 Desmond Molecular Dynamics System, Schrodinger LLC, D.E. Shaw Research, New York, NY, USA, 2023.

[71] W.L. Jorgensen, J. Chandrasekhar, J.D. Madura, R.W. Impey, M.L. Klein, Comparison of simple potential functions for simulating liquid water, J. Chem. Phys. 79 (1983) 926–935, https://doi.org/10.1063/1.445869.
[72] U. Essmann, L. Perera, M.L. Berkowitz, T. Darden, H. Lee, L.G. Pedersen, A smooth particle mesh ewald method, J. Chem. Phys. 103 (1995) 8577–8593, https://doi.org/10.1063/1.470117.
[73] G. Çelik, G. Kılıç, Ş. Kanbolat, S.Ö. Şener, M. Karaköse, N. Yaylı, Ş. Alpay Karaoğlu, Biological activity, volatile and phenolic compounds from five Lamiaceae species, flavour, Fragr. J. 36 (2) (2021) 223–232, https://doi.org/10.1002/ffj.3636.
[74] S.R. Wang, H.Y. Huang, L. Wei, L.Y. Wu, W. Xiong, T. Tian, X. Zhou, The manipulation of RNA-guided nucleic acid cleavage with ninhydrin chemistry, Adv. Sci. 7 (2020) 1903770, https://doi.org/10.1002/advs.201903770.
[75] J.S. Morse, T. Lalonde, S. Xu, W.R. Liu, Learning from the past: possible urgent prevention and treatment options for severe acute respiratory InfectionsCaused by 2019-nCoV, ChemBioChem 21 (2020) 730, https://doi.org/10.1002/cbic.202000047.
[76] L. Zhang, D. Lin, X. Sun, U. Curth, C. Drosten, L. Sauerhering, S. Becker, K. Rox, R. Hilgenfeld, Crystal structure of SARS-CoV-2 main protease provides a basis for design of improved α-ketoamide inhibitors, Science 368 (6489) (2020) 409–412, https://doi.org/10.1126/science.abb3405.
[77] A. Cerda, M. Rivera, G. Armijo, C. Ibarra-Henriquez, J. Reyes, P. Blázquez-Sánchez, Avilés, J.A. Arce, A. Seguel, A.J. Brown, Y. Vásquez, M. Cortez-San Martín, F. A. Cubillos, P. García, M. Ferres, C.A. Ramírez-Sarmiento, F. Federici, R. A. Gutiérrez, An Open One-Step RT-qPCR for SARS-CoV-2 detection, medRxiv (2023), https://doi.org/10.1101/2021.11.29.21267000.
[78] N. Sitaropoulou, E.P. Neophytou, G.N. Thomopoulos, Structure of the nucleocapsid of a filamentous virus of the honey bee (*Apis mellifera*), J. Invertebr. Pathol. 53 (3) (1989) 354–357, https://doi.org/10.1016/0022-2011(89)90099-2.
[79] L. Gauthier, S. Cornman, U. Hartmann, F. Cousserans, J.D. Evans, J.R. de Miranda, P. Neumann, The Apis mellifera filamentous virus genome, Viruses 9 (7) (2015) 3798–3815, https://doi.org/10.3390/v7072798.
[80] S.W. Park, D.M. Cornforth, J. Dushoff, J.S. Weitz, The time scale of asymptomatic transmission affects estimates of epidemic potential in the COVID-19 outbreak, Epidemics 31 (2020) 100392, https://doi.org/10.1016/j.epidem.2020.100392.